A Thesis

entitled

Experimental and Theoretical Investigation of Evaporative Drying Patterns of Manganese Oxide Laden Droplets

by

Clement Dzifa Kekessie

Submitted to the Graduate Faculty as partial fulfillment of the requirements for the

Master of Science Degree in Mechanical Engineering

_____

Dr. Anju Gupta, Committee Chair

_____

Dr. Adam Schroder, Committee Member

_____

Dr. Thehazhnan Ponnaiyan, Committee Member

_____

Dr. Barry W. Scheuermann, Interim Dean
College of Graduate Studies

The University of Toledo

May 2021

An Abstract of

Experimental and Theoretical Investigation of Evaporative Drying Patterns of Manganese Oxide Laden Droplets

by

Clement Dzifa Kekessie

Submitted to the Graduate Faculty as partial fulfillment of the requirements for the Master of Science Degree in Mechanical Engineering

The University of Toledo
May 2021

Droplet evaporation and the resultant patterns provide a fundamental understanding of deposition of multiscale particles suspended in solutions. One of the significant applications of studying evaporative patterns is the inkjet printing which is deemed as an ideal method for deposition of conductive nanomaterials for the fabrication of flexible device.

This work examines the drying pattern of manganese oxide droplets post evaporation. A variety of governing parameters such as substrate temperature, substrate wettability, surface tension and particle concentration were investigated. It was observed that both hydrophobic and hydrophilic substrates maintained at room temperature rendered coffee-rings with uniform distribution of particles at both low and high concentrations. Similar coffee rings patterns were formed on hydrophilic substrates and base fluid comprising of 90/10 (DI water/ethanol). However, on hydrophobic surfaces, rings with an inner deposit of particles were obtained. Additionally, the patterns observed with both hydrophobic and hydrophilic surfaces heated at 50° C resulted showed predominantly ring-like patterns with

uniform distribution of particles with the only difference being the variation in ring thickness.

I dedicate this thesis to my mom, sister and my uncle for their love and support throughout my graduate school journey.

Acknowledgements

I would like to express my gratitude to my advisor Dr. Anju Gupta for her guidance on this research. And my lab mates for their assistance and encouragement when I needed it the most.

Table of Contents

List of Tables

List of Figures

List of Abbreviations

CA .....Contact angle
CAH .....Contact Angle Hysteresis

CCA .....Constant Contact Angle
CCR.....Constant Contact Radius

DI .....Deionized Water
DLVO .....Derjaguin-Landau-Verwey-Overbeek interactions

ICRDs .....Inner Coffee-ring Deposits

OLED.....Organic Light-Emitting Diode

PEG.....Poly(ethylene glycol)
PEO.....Polyethylene Oxide
PMMA .....Poly (methyl methacrylate)
PTFE .....Polytetrafluoroethylene

SDS .....Sodium Dodecylsulfate

TCL.....Triple Contact Line

XO.....Xanthan Gum

List of Symbols

γ_{sv} .....Solid-Vapor Surface Tension
γ_{sl} .....Solid-Liquid Surface Tensions
k_S .....Substrate Conductivity
k_L .....Liquid Conductivity
k_R ..... The Heat Flux at The Liquid/Substrate
λ_c .....Capillary Length
T_s .....Substrate Temperature

α .....Thermal Diffusivity
η .....Dynamic Viscosity
σ .....Surface Tension
γ ..... Liquid Surface Tension
ρ .....Density of the Droplet

Ma .....Marangoni Number
θ .....Contact angle
T..... Temperature
l .....Length
R.....Contact Radius of Sessile Droplet
V.....Volume of Sessile Droplet
S .....Surface Area of Sessile Droplet
h.....Height of Sessile Droplet
g.....Gravitational Constant

Au.....Gold
Al_2O_3 .....Aluminium Oxide
CuO .....Copper Oxide
H2O.....Water
MnO_2.....Manganese Oxide
δ-MnO_2.....Birnessite
SiO_2 .....Silicon
TiO_2.....Titanium Oxide
O_2 .....Oxygen
NaCl .....Sodium Chloride

Chapter 1

Introduction and literature review on colloidal droplets

1.1 Modes of Droplet Evaporation studies: Importance and applications

The difference of liquid concentration gradient and physical properties of a liquid, like density, diffusion coefficient in air, molecular weight and heat of vaporization control droplet evaporation [1]. Droplet evaporation plays an important role in various industrial and biological applications including inkjet printing, hot spot cooling, surface patterning, droplet-based microfluidics, paints, and DNA mapping [2]–[4]. Droplet evaporation also plays a vital role in various fields of natural science and engineering such as: cloud physics, burning liquid-fuels, air/fuel-premixing and (biological) crystal growth [5]. Through, the right modeling of the evaporation of aqueous solutions the efficiency of heat pumps have been increased [6].

The evaporation rate of pure liquids has been studied and it has been observed that the droplet shrinks steadily until it disappears.

In general, droplet evaporation occurs in two stages; it begins with the contact line pinned and the contact angle decreasing during drying [7]. In the second stage, when the contact

angle reaches a critical value, it starts to recede [7]. The initial pinning stage can occupy 90–95% of the droplet lifetime [8]. The evaporation of a droplet is affected by the initial contact angle of the droplet as well as the contact angle hysteresis [9],[10].

Fang et al. [11] observed that during the evaporation of a droplet, depending on the composition of the surface the adsorbing power with respect to water differs and this in turn affects the drying behavior of the droplet [12].

When solid particles are added to a sessile droplet, their interaction with the solid surface during evaporation results in the formation of different deposited patterns due to adsorption of particles at the liquid-vapor interface [13]. For an evaporating droplet dispersed with colloidal particles the non-uniform evaporation flux along the liquid–gas interface is largest near the contact line which causes the outward capillary fluid flow of particles toward the contact line which results in the "coffee-ring" pattern [14].

Two important flow fields widely accepted as responsible for the formation of patterns in these colloidal droplets are the Capillary flow and Marangoni flow. Marangoni flow is a convection flow that is driven by the surface tension gradient in the droplet, this flow can arise due to concentration gradient or Solutal Marangoni effect or a temperature gradient also known as the thermal Marangoni effect [15],[16].

Researchers have found that Solutal Marangoni effect can be created by the addition of surfactants which induces the concentration gradients in a drying droplet that leads to a surface tension gradient along the free surface [17],[18]. The increase in substrate temperature has also been found the increase thermal Marangoni effect which ultimately influence pattern formation in colloidal droplets [19].

Features such as the rate of drying, wettability and the final pattern formed, depend on a number of parameters [2],[20] such as surfactant concentration [17],[18], ambient pressure [21], pH of the colloidal suspension [22], shape of the particles [23].

This study qualitatively studied the effect of substrate temperature, substrate hydrophilicity and hydrophobicity, particle concentration and base fluid formation on manganese oxide (MnO_2) laden droplets. Optical microscopy was employed to observe the evaporation process of the MnO_2 laden droplets from the top view. Sequential images were taken, and experimental results were analyzed based on the results from literature on the evaporation of droplets containing other colloidal particles [24]–[27].

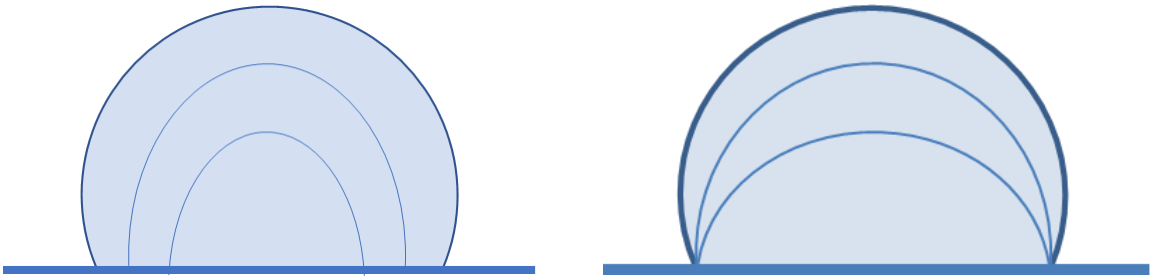

Figure 1-1: The modes of evaporation (a) Constant Contact Angle (CCA) mode and (b) Constant Contact Radius (CCR) mode

1.1.1 Modes of Droplet Evaporation

Picknett and Bexon [28] identified two modes of evaporation of a droplet resting on a smooth homogeneous surface, namely, the constant contact angle (CCA) mode and the constant contact radius (CCR) mode.

i. The *constant contact angle (CCA) mode*, the contact angle and the spherical cap shape does not change but only the contact area between the liquid and solid changes.

ii. The *constant contact radius (CCR) mode* due to contact angle hysteresis during evaporation the contact area between the liquid and solid as well as the spherical cap shape does not change but only the contact angle.

iii. The *mixed mode* has also been reported where after evaporation through the CCR and CCA modes is followed by the mixed mode; both the contact angle and the contact radius decrease simultaneously [29]–[32].

Bourges-Monnier and Shanahan [33] observed four distinct stages in the evaporation of a sessile droplet. During stage 1 the contact radius remains constant while the contact angle and drop height decrease during Stage 2. Stage 3, the drop height and contact radius diminish simultaneously at constant contact angle and finally in Stage 4 corresponds to the evaporation of the remaining liquid.

The *"stick slip" mode* has also been reported [34], in which the wetting front remains static for most of the time the CCR mode corresponding to a "stick" phase, the contact line then slips into a new position leading to a smaller contact radius when the contact angle reaches a threshold corresponding to a "slip" phase. After this the droplet "stick" again until the next depinning occurs. The "stick" phase accounts for the majority of the droplet lifetime, but the "slip" phase occurs quickly. This cycle of the "stick" and "slip" phases repeats till the complete evaporation of the droplet.

During the stick-slip mode sessile droplet is in a thermodynamic equilibrium, the free surface/interfacial energies of the system is at its minimum level [31],[32]. The decrease

in the contact angle of the pinned droplet leads to the increase of this free energy above an energy barrier and the contact line slips to a new equilibrium position to dissipate the excess free energy [35],[36].

Uno.et al. [37] found that the droplet evaporation followed CCR mode on a hydrophilic surface, but follows the CCA mode on a hydrophobic surface.

1.2 Literature review on Pattern Formation During Droplet Evaporation

In this section, various patterns that have been reported in literature in the study of evaporating colloidal droplets are discussed.

1.2.1 Coffee-ring Pattern

Coffee-ring pattern occurs due to the non-uniform evaporation flux on the droplet surface, which causes the liquid within the droplet to flow outward the edge when the Marangoni effect is negligible to compensate the large evaporation loss of liquid at the edge [14],[38]. It has been found from previous studies that the necessary conditions for formation of the coffee stain are; one the evaporation of liquid [14], two the fact that the drop should be pinned to the substrate during evaporation [14] and three the suppression of Marangoni flow [16].

Hu and Larson [16] demonstrated that the coffee-ring pattern does not only form due to a pinned contact line and continuous evaporation of liquid, but also the suppression of a Marangoni flow is also required. They found that Marangoni flow induced by the surface tension gradient resulting from the evaporation deposited some particles the central region

of the droplet. Therefore, the Marangoni flow should be either reduced or eliminated to create the coffee-ring pattern.

Shen et al. [39] showed that there exists a lower limit of droplet size, for the formation of a coffee ring structure. They demonstrated that when the liquid evaporates much faster than the particle movement, coffee ring formation may cease as the particles do not have enough time to reach the contact line to form a deposit.

For suspended particles of approximately 10 nm, the minimum diameter of the droplet with the coffee-ring pattern was found to be 100 μm.

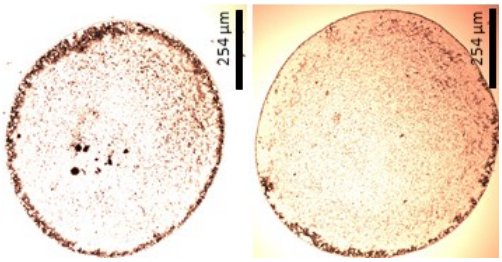

Figure 1-2: An image of a coffee-ring pattern demonstrating distribution of particles along the edges of the drying spot

1.2.2 Uniform Pattern

For application such as ink-jet printing [40], surface coatings [41] and bioassays [42], a uniform deposition of patterns is required rather than a coffee-ring pattern. Colloidal droplets with high concentration of particles may leave a ring-like pattern but with the uniform distribution of particles in the region enclosed by the ring [43],[44].

Seo et al. [42] reported yielding multi-ring pattern over a droplet area using Polyethylene glycol (PEG) to break the coffee-ring effect and obtained a uniform deposition. The addition of PEG in the droplets caused a surface tension variation that induced a centripetal Marangoni flow which successfully altered the coffee-ring effect. Majumder et al. [38]

showed that uniform deposition of nanoparticles in aqueous suspensions could be attained altering the surface tension of the fluid. On hydrophilic substrate the Marangoni forces generated by the surface tension gradient within a droplet on a prevents particles from accumulating at the pinned edge and transports them towards the top of the droplet along the air-liquid interface. The inward Marangoni flow keeps the particles from accumulating at the contact line which inhibits coffee-ring formation and forms a uniform pattern.

Controlling particles interactions within a droplet and the evaporation can help form a uniform pattern [45]–[47].

Li et al. [46] reported that if the droplet dries rapid enough, particles tends to accumulate at the air-liquid interface rather than at the drop edge and directly deposit in the interior. Hence, by controlling the evaporation kinetics uniform deposition can be achieved.

Bhardwaj et al. [22] altered the particle-particle and particle-substrate interactions due to variation of solution pH. The Derjaguin-Landau-Verwey-Overbeek (DLVO) force were found to be attractive at low pH, and the particles close to the substrate are attracted to the center to form a ring pattern with a thick uniform deposition of particles in the interior of the ring. At intermediate pH, particles aggregated at the initial wetted area due to stronger particle-particle interaction but smaller DLVO force between the particles and the substrate. However, a ring pattern was formed with almost all particles deposited in a periphery of the ring at high pH due to the strong repulsive particle-substrate interaction.

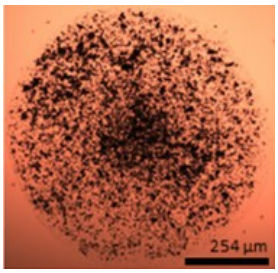

Figure 1-3: A view of a uniform pattern demonstrating uniform distribution of particles

1.2.3 Crack Pattern

Residual stress release from colloidal films made by the evaporation of colloidal droplets containing nanoparticles is responsible for crack formation [48]. Prevention of these cracks is necessary for applications like coatings [49].

Kim et al. [48] used confocal laser microscopy to study crack generation in colloidal droplets. They found that crack generation is dependent on the particle size and initial concentration. They suggested that by controlling the colloid polymer interactions by mixing a nonadsorbing polymer with the colloidal suspension crack formation can be prevented.

The evolution of the drop shape depends on the salt content, thus the morphology of crack patterns are different for various salt contents [49],[50].

Pauchard et al. [49] studied the influence of salt content on crack patterns formed during the desiccation of a colloidal suspension. Radial cracks regularly formed at the drop edge for low salt content, while a disordered crack pattern formed at intermediate salinities, the observed disordered crack pattern was related a buckling instability. At large salt contents, a unique circular crack pattern was formed.

Zhang et al. [51] studied the cracking behavior of polytetrafluoroethylene (PTFE) colloidal droplets. They observe that due to the stretching effect of the liquid zone leads to the build-

up of a macroscopic stress field which determines the final radialized distribution of cracks. The thickness of the film determines the propagation velocity of the cracks depends. In addition, they noted that sodium dodecylsulfate (SDS) additives can be used to tune crack behavior by causing a reduction of the capillary force between particles.

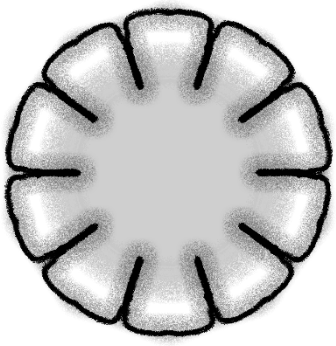

Figure 1-4: A view of cracks shown to be developed on the droplet periphery

1.2.4 Fingering Pattern

Residual stress release from colloidal films made by the evaporation of colloidal droplets containing nanoparticles is responsible for crack formation [48]. Prevention of these cracks is necessary for applications like coatings [49].

Kim et al.[48] used confocal laser microscopy to study crack generation in colloidal droplets. They found that crack generation is dependent on the particle size and initial concentration. They suggested that by controlling the colloid polymer interactions by mixing a nonadsorbing polymer with the colloidal suspension crack formation can be prevented.

The evolution of the drop shape depends on the salt content, thus the morphology of crack patterns are different for various salt contents [49],[50].

Pauchard et al. [49] studied the influence of salt content on crack patterns formed during the desiccation of a colloidal suspension. Radial cracks regularly formed at the drop edge for low salt content, while a disordered crack pattern formed at intermediate salinities, the observed disordered crack pattern was related a buckling instability. At large salt contents, a unique circular crack pattern was formed.

Zhang et al. [51] studied the cracking behavior of PTFE colloidal droplets. They observe that due to the stretching effect of the liquid zone leads to the build-up of a macroscopic stress field which determines the final radialized distribution of cracks. The thickness of the film determines the propagation velocity of the cracks depends. In addition, they noted that sodium dodecylsulfate (SDS) additives can be used to tune crack behavior by causing a reduction of the capillary force between particles.

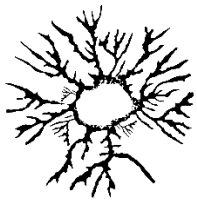

Figure 1-5: Fingering pattern demonstrating the fingering phenomenon

1.2.5 Stick-slip Pattern

The stick slip pattern occurs when particles stick to the contact line during the initial evaporation stage and recedes “slips” to another position and particles again form another ring.

Orejon [43] reported the several pinning-depinning cycles, known as “stick-slip” behavior in droplets containing TiO_2 nanoparticles on hydrophobic substrates. They reported that increasing concentration resulted in a higher number of nanoparticles reaching the contact

line which increases the local energy barrier, and this results in a profound "Stick-slip" behavior. The "stick" phase of the "stick-slip" mode corresponds to nanoparticles accumulating at the triple contact line to form a ring and the "slip" corresponds to a jump of the contact line, and the consequent change in contact angle. This behavior was observed to continue until the complete evaporation of the TiO_2 nanofluid.

Moffat et al. [52] also noticed that distinct "stick-slip" pinning behavior of the triple line occurred when nanoparticles were added to the base liquid and increased nanoparticle concentration enhanced the "stick-slip" behavior. The observed behavior was attributed to the effects of particle accumulation near the contact line, caused by the now advective flow during evaporation.

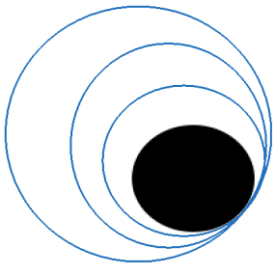

Figure 1-6: The stick-slip pattern demonstrating the stick-slip behavior from a drying droplet

1.2.6 Crystal Pattern

Most studies has stipulated that crystalline patterns are often observed in the central regions of the dried droplets containing salts [50],[53]–[58].

Gorr et al. [50] studied the effect of sodium chloride (NaCl) concentrations on evaporation aqueous lysozyme sessile droplets. The patterns formed on the substrate show significant dependence on initial NaCl concentration. With lysozyme solutions of less salt concentration, the remaining liquid in the central region depins and recedes until complete

evaporation of the droplet whiles those with higher salt concentrations, the contact angle continues to decrease while the remaining liquid evaporates. In the final stages of evaporation, there is the formation of cracks in the perimeter ring. They found that three regions are generally formed; Region I consist of a lysozyme-rich amorphous peripheral ring, Region II consist of a secondary ring-like area consisting of larger lysozyme aggregates, and Region III is the central region which contains dendritic and cubic crystallites. With increasing NaCl in solution, the width of the ring decreases.

Zhong et al. [58] studied the evaporative dynamics and crystalline patterns on silicon wafer, poly(methyl methacrylate) (PMMA) plate and soda lemon glass substrates for saline droplets. On the silicon wafer and PMMA plate, higher salt concentration resulted in the continuous increase of the contact angle in the middle of evaporation. Due to the lower wettability and the smaller pinning effect of silicon wafer and PMMA substrates, the morphology of patterns formed were either comprised of either a single cube or accumulated crystals at the droplet center. On the other hand, the soda lemon glass showed high wettability and longer pinning effect and the resulting crystalline deposit depended greatly on the salt concentration. For low salt concentrations, exterior cracked layers of salt developed at the contact area between the substrate and droplet and interior separated small crystal cubes, whereas large crystalline chunks stay near the droplet rim for high salt concentrations.

Kaya et al. [55] studied the of drying aqueous drops of sodium poly(styrene sulfonate) containing fixed amounts of sodium chloride. Crystallization of salt molecules takes place at a critical concentration and they observed patterns include concentric rings, needle-like structures, chains of triangular-shaped crystallites. The addition of polymer into the saline

solutions on low wettability substrates promoted the pinning effect and prevented the formation of single square-shaped crystals in the centre of the dried droplets.

Giri et al. [53] found that NaCl forms crystalline patterns during desiccation in different gel type solvents. In gelatin, it forms the usual cubic crystals of macroscopic dimensions, but in the regions in between, it forms highly intricate ramified dendritic patterns with a 4-fold symmetry, visible under a microscope.

Chen et al. [54] studied micro structured protein patterns and found that, no protein patterns were formed upon complete evaporation of a salt-free protein aqueous solution. With the increase of salt concentration, scalloped and rosette-like protein patterns were obtained and as the salt concentrations further increased to more than 1M, regular, well-organized protein patterns were disrupted by the crystallized salts. With the increase in protein concentration, the deposited protein patterns changed from the sparsely distributed starlike shape to the beautiful rosette shape.

Shahidzadeh-Bonn et al. [56] observed that sodium chloride crystals are found to form preferentially in contact with a nonpolar area while hydrated sodium sulfate and anhydrous sodium chloride crystals were observed to form at the liquid-vapor interface of both the meniscus within the tube and in the thick wetting films in the corners.

Figure 1-7: Crystal patterns as observed in the central regions of dried droplets

1.2.7 Combined Pattern

Nguyen et al. [59] observed inner coffee-ring deposits (ICRDs) after the evaporation of sessile water droplets containing silica nanoparticles and organic pigment nanoparticles.

They observed that the radius of ICRDs decreased initially and increased with increasing concentration of added salts and nanoparticles and with increasing contact angle hysteresis of hydrophobic surfaces. Different dendrite deposit patterns inside ICRDs we also observed. All these deposit patterns were attributed to the second pinning of the three-phase contact lines, which occur when the forces on particles are balanced.

Crivoi and Duan [60] reported the formation well-distinguished branched structures inside the coffee ring left after the full drying of a water-based copper nanofluid droplet. They found that this combined pattern was due to the nucleation and growth process inside the peripheral ring.

Li et al. [61] reported that on substrate possessing weak contact angle hysteresis (CAH) with respect to pure water

a combined pattern of a ringlike and concentrated stain can appear for a mixture of surface-active and surface inactive solutes such as Brij-35 and $CoSO_4$. The pinned contact line induced by surfactant adsorption during the final stage of drying and the occurrence of surfactant precipitation leads to the formation of the ringlike stain. When the depinning of the contact line started from a corner, most parts of the contact line receded towards the part that has been pinned throughout and as the precipitation of surface-inactive solutes takes place in the vicinity of the pinned contact line, and the concentrated stain is developed.

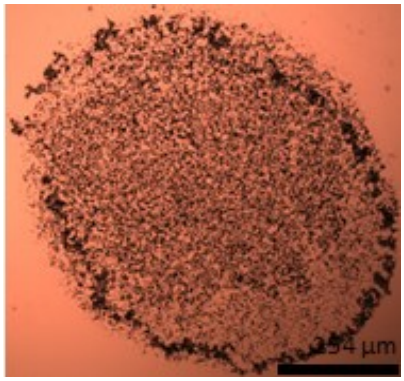

Figure 1-8: A coffee-ring pattern with uniform distribution of particles inside the ring

1.3 Particle laden droplets: Applications of manganese oxide particles

The ability of manganese oxides to change their structure and bonds them makes ideal for electronic and magnetic applications [62]. Manganese oxides have been used in different applications, like electrodes for rechargeable lithium batteries, catalysts, soft-magnetic materials, high-density magnetic storage media, sensors, supercapacitors, electronics, adsorbent for metal ions and contaminant clean-up from wastewater [63]–[67]. Various synthesis routes has been discussed for the preparation of manganese oxide nanomaterials of different morphologies, such as Inert gas condensation, Chemical vapor synthesis, Coprecipitation, Sol-gel synthesis, Microemulsion, Wet Chemical route, Sonochemical methods, Hydrothermal/Solvothermal Processing, Solid state techniques [62],[68]–[70].

Dastjerdi et al. [71] investigated the adsorption behavior of manganese oxide nanowires as an adsorbent for the removal of dissolved toluene from underground water. The porous nanowire membrane which has a superhydrophobic character, is very suitable for removal

of the hydrophobic molecules. The results of this study suggest that nanowires of manganese oxides can be used as a low cost, highly efficient adsorbent for the removal of dissolved hydrocarbon from aqueous solution.

With inkjet printing-based industrial applications such as microelectronics and display systems understanding the deposition mechanisms of nanoparticles in droplets on a substrate is of extreme importance.

Thokchom et al. [3] studied the underlying mechanisms of the self-assembly and deposition behavior of nanoparticles in inkjet-printed, evaporating droplets by visualizing the internal fluid flows. They verified that Marangoni flow generated on the Polydimethylsiloxane (PDMS) substrate helps the formation of dome-shaped nanoparticle structures, while radially outward flow generated on the glass substrate pro-duces either mono-layered and flat, or ring-shaped nanoparticle structures, depending on the number density of the suspension.

On the other hand, the application of Inkjet printing based on ink formulations of MnO_2 nanosheets with desired patterns has been possible for different applications [72]–[74].

According to Elshof and Wang [72], the physical properties and storage stability of printable nanosheet-based inks can be improved by additives such as surfactants and/or thickeners. They also stated that the average lateral nanosheet size of inkjet printed electrochemical energy storage devices needs to be optimized to get the best electrochemical performance.

Inkjet printing has been used to fabricate flexible electronic devices like field effect transistors [75],[76], solar cells [77],[78], and electrochemical energy storage devices [74].

Wang et al. [74] were able to fabricate a micro-supercapacitor using a highly concentrated ink containing two-dimensional δ-MnO2 nanosheets with an average lateral size of 89 nm and around 1 nm thickness. They were able to engineer the formulation of the δ-MnO_2 ink, and inkjet printed it on an O_2 plasma treated glass and polyimide film substrates to form δ-MnO_2 patterns without undesired "coffee-ring" effect.

Studying the deposited patterns of manganese oxide laden droplets, we believe would help understand how to formulate inks that can produce the desired patterns for application in inkjet printed flexible microelectronics.

1.4 Factors that influence deposited patterns

During evaporation of liquid droplets on solid substrates an exchange of mass and energy between phases takes place. This depends on many factors such as; substrate wettability [85], particle size [79], surface hydrophilicity and hydrophobicity [80], surface temperature [81] and particle concentration [36] amongst others that can be manipulated to control the patterns formed.

1.4.1 Effects of substrate wettability (hydrophilicity and hydrophobicity)

In the case of pure fluids, on hydrophobic substrates evaporation is reported to occur at constant contact angle (CCA) mode, while on hydrophilic substrates, droplet evaporation proceeds at constant contact radius (CCR) leading to a steady rate of evaporation over time [4],[82]. On most hydrophilic substrates an initial pinning of the contact line followed by either a continuous or an interrupted receding of the contact line was observed, on glass for instance, where there is no depinning of the contact line and a constant evaporation rate was reported

during most of the droplet lifetime, in contrast to hydrophobic substrates where continuous receding of the contact line is reported [33],[83]–[86].

On hydrophobic surfaces the addition of nanoparticles to a base fluid modifies the evaporative behavior leading to a "stick-slip" behavior [87],[88]. Heating can change the stick or slip behavior of particles in a solution depending on whether the substrate is hydrophilic or hydrophobic [37], [80],[89].

Shanahan et al. [87] reported that for a given droplet volume, evaporation on hydrophilic substrates proceeds quicker due to lower equilibrium contact angle and therefore greater base radius than that adopted on hydrophobic ones. Since evaporation rate is proportional to the base radius, shorter timescales are observed for droplet evaporation on hydrophilic substrates when compare to low energy ones.

Nguyen et al. [59] obtained centralized deposits on a salinized hydrophobic silicon substrate, due to the depinning of the contact line which brings silica particles to the inner region of the droplet. Li et al. [61] controlled polymer nanoparticle deposition by varying the contact angle hysteresis (CAH) of the substrates. They reported centralized deposits for weak CAH substrate (such as sodium polysulfonate) and ring-like patterns on strong CAH substrates (such as polyvinylpyrrolidone).

Chhasatia and Sun [90] investigated the deposition behavior of an inkjet-printed aqueous colloidal drop consisting of bi-dispersed micro- and nanoparticles. For a hydrophobic substrate, the constant contact angle stage dominates the entire evaporation process, and this does not leave room for particles to rearrange according to their sizes such that micro- and nanoparticles mix well in the final deposition. For a hydrophilic substrate, particle separation is incomplete in the final deposition. This was attributed to the effects of the different evaporation modes, the

substrate-particle interactions, the surface tension and drag forces acting on particles on the rearrangement of particles near the contact line during evaporation.

Studies has shown that increasing hydrophobic substrate temperature led to the transition from the dot-like pattern to the inner deposit inside the peripheral ring [25],[80],[81]

1.4.2 Effects of substrate temperature

Varying substrate temperatures can suppress the coffee-ring effect by varying the surface tension gradients of the liquid–gas interface [25],[81]. This bring about Marangoni flows induced thermal Marangoni stresses at the liquid–gas interface due to non-uniform cooling of the interface by latent heat of evaporation which reverses the outward capillary flow of particles and changes the particle deposition from the ring to the droplet center region [15],[91].

Patil et al. [80] studied the effect of substrate heating (T_s = 27–90°C) on hydrophilic glass and hydrophobic silicon of evaporation of droplets containing polystyrene particles with different particle concentrations, 0.05, 0.1 and 1.0% (v/v). At ambient, a ring and an inner deposit formed on glass and silicon, respectively but at higher substrate temperature, a thin ring with inner deposit formed on both substrates. The drying process occurred mostly in the CCR mode due to the self-pinning of particles in the stagnation region. This resulted in the thin coffee-ring pattern formed on the heated substrate with the inner deposit inside the ring.

Xu et al. [92] showed that the thickness of substrate influences the temperature gradient on the liquid−gas interface and direction of Marangoni convection.

Zhong et al. [19] varied substrate temperature of nanofluid droplets of graphite nanopowders from 22-84°C on silicon substrates and observed a distinct “dual-ring”

pattern. Increasing the substrate temperature resulted in the "dual-ring" pattern disappearing and formed a single ring pattern. They found that enhancing the temperature increased the inward Marangoni flow along the liquid-vapor interface which carried nanoparticles inward and at the same time, the enhanced capillary flow expanded the inner ring and merged it with the outer ring.

Parsa et al. [25] varied surface temperature from 25-99℃ using nanofluids of copper oxide nanoparticles where they noticed a change from a uniform particle deposition to a dual-ring pattern. This was due to higher evaporation rate at higher temperatures which enhances nanoparticle velocity. Thus stick-slip pattern developed at the highest temperature 99℃ due to nanoparticles arriving more rapidly at the depinned triple line leading to a larger secondary ring. Later, Parsa et al. [26] also studied the deposition patterns of binary water-butanol CuO nanofluid droplets. Similar to the patterns observed for the water-based droplets [25], the nearly uniform pattern was formed on the non-heated substrate, the "dual-ring" patterns for heated substrate temperatures from 47 to 81℃, and the "stick-slip" pattern for substrate temperature of 99℃. However, unlike the evaporation of CuO-water droplets, the distribution of nanoparticles was found to be different as several inner faint lines were observed inside the secondary ring of the "dual-ring" patterns.

Li et al. [81] reported the effect of temperature on patterns formed after the evaporation of droplets of polystyrene particles on heated substrates. The coffee ring pattern changes to a "coffee eye", that is, a thin peripheral ring with an inner deposit at the center due to higher Marangoni flow arising from temperature differences between the droplet edge and the apex when the substrate temperature is elevated.

Zhong and Duan [93] studied droplets of graphite nanopowders with varying surface temperature from 10-50°C. The deposited patterns are shown to vary from a uniform disk-like profile to a dual ring from cooling to heating of the substrate with increase in substrate temperature.

Chon et al. [79] tested nanofluids containing CuO, Au and Al_2O_3 nanoparticles. The nanofluid droplets show strong pinning along the droplet perimeter and, upon evaporation, leave a ring-shaped nanoparticle stain. Particle size had a strong effect on the dryout stain pattern, while heater temperature seems to have little effect. They reported that due to the large difference of thermal conductivity between nanoparticles and water, the temperature span between the droplet center and edge increases with increasing particle size but for smaller nanoparticles, it decreases.

In all the above studies the thinning of the ring and formation of either inner deposit or the dual ring were attributed to the increase in substrate temperature which leads to Marangoni convection inside the droplet that transports the particles from the contact line region to the inner region of the droplet.

1.4.3 Effects of particle concentration

Anyfantakis et al. [94] To test this scenario, we used aqueous suspensions of fumed silica nanoparticles (NPs) of varying wettabilities. For hydrophilic NPs, the dry patterns always had a ring-shaped morphology for all particle concentrations investigated. For suspensions containing NPs of lower wettability, the particle concentration had a strong influence on the dry pattern morphology. As the hydrophobicity of the NPs increased, they observed a general ring → mixed ring/thick disk → thick disk → dome deposit evolution.

For dilute suspensions, ring-shaped deposits were obtained for the whole particle wettability range

examined. For intermediate particle concentrations, a ring → thick disk → flattened dome evolution occurred. At high solid contents, a ring → flattened dome → steep dome progression was observed. For suspensions containing nanoparticles of lower wettability, the particle concentration had a strong influence on the dry pattern morphology and also Karapetsas et al. [95] noted that for particle-laden droplets and in the case of dilute solutions, the droplet life-time is found to be weakly-dependent on the initial particle concentration.

Orejon et al. [36] showed that the particle concentration influences the depinning of the contact line on nonheated, hydrophobic substrate; they found a correlation between the distance jump by the contact line and nanoparticle concentration for instances, higher concentration leads to a longer pinning of the contact line, which leads to a large deviation in contact radius before the jump. Increasing nanoparticle concentration was found to enhance the "stick-slip" behavior [96].

Brutin [97] studied the effect of polystyrene nano-particle concentration and observed that the patterns formed were influenced mainly by the concentration of nano-particles but not not the drying time. An o-ring with no particles in the interior ring at concentrations below 0.47% and a flower pattern was formed above 1.15%. The number of nanoparticles deposited increased with increasing concentration, whereas the number of "flower petals" decreased with concentration.

Sefiane [98] studied the effect of concentration on Al_2O_3-H_2O and TiO_2-H_2O nanofluids where it was observed for all concentrations that a ring-like patterns were formed and the

thickness of the ring increased with increasing concentration. A comparison between Al_2O_3 and TiO_2 nanofluids show that, Al_2O_3 enhances pinning more than TiO_2 for the same concentrations on similar substrates.

Lee et al. [99] studied the effects of particle size and concentration of Al_2O_3 and TiO_2 nanofluid droplets on different substrates (glass, stainless steel and Teflon). At low concentrations and small particle sizes, a ring-shaped pattern was formed, while a uniform pattern was formed at high concentrations and large particle sizes for Al_2O_3 nanofluids. On the contrary, only ring-shaped patterns were observed for all concentrations of TiO_2 nanofluids.

1.4.4 Effects of surface tension (Base fluid)

The nature of the base fluid and its composition can affect the internal flow and the evaporative dynamics of an evaporating droplet and consequently influence the morphology. Base fluid plays an important role in the formation of deposition patterns.

Choi et al. [100] studied the pattern formation of polystyrene particles suspended in aqueous solutions of water, Polyethylene Oxide (PEO), and xanthan gum (XG). The XG solution formed the coffee-ring pattern, while the water and PEO solutions formed a more inner uniform pattern with no distinct ring. The difference in viscosities between the PEO and XG solutions resulted in the deposition patterns observed. The base fluid with higher viscosity formed the coffee-ring pattern, while the lower viscosity fluids formed a more uniform pattern.

Zhong and Duan [27] studied the evaporation dynamics of graphite−water nanofluid droplets. They found that deposition patterns of water-ethanol binary-based nanofluid droplets are affected by the ethanol concentration. Increasing ethanol from 0 to

50 vol% promoted the uniformity of the deposited patterns. The pure water-based suspension formed a nearly uniform pattern. However, when 10 vol % ethanol was added, most nanoparticles deposited in the center of the droplet and detached from the peripheral ring. At 25 vol % ethanol concentration, the pattern showed uniformity again. Finally, the inner deposit started to detach from the peripheral ring with a further increase of the ethanol concentration to 40 and 50 vol %. This was attributed to the strong fluid circulation that carried nanoparticles to the interface and form aggregate which was not observed in the water-based droplets.

Talbot et al. [101] studied deposited patterns from colloidal droplets base on the two binary fluids of water-ethylene glycol and water-ethanol. For water-ethylene glycol binary fluids at low concentrations (10 and 30 vol %) uniform patterns enclosed with thick rings were formed while at higher concentrations of ethylene glycol (50 – 90 vol %), ring-like patterns were formed with the less dense interior regions. At high concentration of ethylene glycol, no inward Marangoni flow was observed, a slow radial flow dominated the evaporation, leading to the formation of the rings with unfilled regions inside the peripheral rings. The water-ethanol droplets formed ring-like deposits and the width of the rings increased with increasing ethanol concentration from 10 to 90 vol %.

Parsa et al. [26] studied the deposition patterns of binary water-butanol CuO nanofluid droplets. Adding 5 wt % butanol into the base fluid did not significantly affect the deposition patterns. On the non-heated substrate a nearly uniform pattern was formed, for the heated substrate temperatures from 47 to 81℃, a "dual-ring" patterns were formed, and the "stick-slip" pattern was observed for the substrate temperature of 99℃.

Similar to the evaporation behavior of the pure liquid droplets reported by Sefiane et al. [102], Cheng et al. [103], and Liu et al. [104], Zhong and Duan [27] noticed the droplets with graphite nanoparticles evaporate faster with an increase in the ethanol concentration. The evaporating droplets with relatively low ethanol concentrations remain pinned, while those at 40 and 50 vol % of ethanol exhibit a depinning behavior at the late stage. With a higher ethanol component, droplets without particles were observed to shrink rapidly from the beginning of evaporation, and then the retraction continued but with a slower rate [102],[103].

1.5 Mathematical parameters of a sessile droplet

The following section summarized mathematical parameters correlating to droplet evaporation.

The competition between the capillary effect leading to the coffee ring and Marangoni effect is decided by several parameters including the thermal conductivities of the substrate and fluid [105]–[108] and a Marangoni number (thermal) has been defined to characterize this [20],[109];

$$Ma = -\frac{\partial \sigma}{\partial T}\frac{l\Delta T}{\eta \alpha} \quad (1)$$

Here, ΔT is the temperature gradient, α is thermal diffusivity m^2/s, σ is surface tension N/m, l length m and η is dynamic viscosity $kg \cdot (m \cdot s)^{-1}$

High contact angle of the liquid on the substrate is needed for getting higher height to induce stronger Marangoni flow inside the droplet.

Analysis indicates that the drop is warmest at the contact line only if the substrate conductivity k_S is at least a factor of 2 greater than the liquid conductivity k_L $k_R \equiv k_S/k_L >$ 2 [110]. In this situation, the consequent Marangoni flow is directed radially outward along the substrate. For 1.45< k_R < 2, the direction of the temperature gradient (and the resulting flow) depends on the contact angle [110].

The surface energy of the substrate and the liquid drop, as well as the interface energies between different phases and the interface free energy that is needed to create an interface between the liquid and solid all determine the shape of the drop on a surface [20]. A sessile drop resting on an ideal, flat, rigid, solid surface presents a contact angle which, at equilibrium, is expected to be given by Young's equation [20],[52]:

$$\gamma_{lv}\cos\theta = \gamma_{sv} - \gamma_{sl} \qquad (2)$$

where γ_{lv} is the liquid surface tension, and γ_{sv} and γ_{sl} are the solid-vapor and solid-liquid surface tensions, respectively, θ is the equilibrium contact angle between liquid and the surface (Figure 1-9).

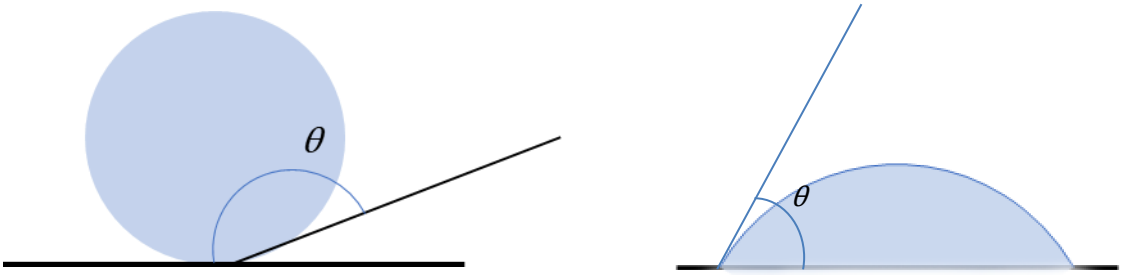

(a) (b)

Figure 1-9: Contact angle between a drop and a substrate [20] (a) Nonwettable substrate (b) Partially wetted substrate

After a colloidal droplet reaches equilibrium, the geometric shape of the sessile drop can be estimated by the capillary length (λc): [20], [111]

$$\lambda_c = \sqrt{\frac{\gamma}{\rho g}} \qquad (3)$$

where γ is surface tension, ρ is the density of the droplet kg/m^3, and g is the gravitational constant m/s^2.

If the contact radius (R) of the sessile drop is less than the capillary length, the gravitational force is negligible; the droplet will form a spherical cap shape. Therefore, the height (h), volume (V) and surface area (S) can be calculated as follows:

$$h = Rtan\frac{\theta^*}{2} \qquad (4)$$

$$V = \frac{\pi R^3(1-cos\theta^*)^2(2+cos\theta^*)}{3sin^3\theta^*} = \frac{1}{6}\pi h(h^2+3R^2) \qquad (5)$$

$$S = \frac{2\pi R^2}{(1+cos\theta^*)} = \pi(h^2+R^2) \qquad (6)$$

1.6 Hypothesis

Manganese oxide particles presents opportunities in various fields of application as highlighted in Section 1.3. The application of Manganese oxide ink formulations for inkjet printing of microelectronics has many interesting prospects. One primary problem is the engineering of the ink formulation and optimizing the drop spacing to avoid the formation of coffee-ring patterns.

Through this study of Manganese oxide laden droplets, we hope to understand the underlying mechanism and conditions necessary for the formation of deposited patterns by investigation the effects of the factors mentioned in Section 1.1.

1.7 Objectives

Evaporation of particle laden droplets of nanoparticles has been extensively studied with the consideration of effects such surface wettability and temperature, particle size, concentration, base fluid, droplet size among others [87]-[104].

The focus of this work is to understand and predict the combined effects of substrate wettability, substrate temperature, surface tension of the liquid and particle concentration of particle laden droplets on both hydrophobic and hydrophilic substrates. With this research we considered the evaporation of droplets of sizes of $1\mu l$ with $5\mu m$ Manganese oxide particles.

This study investigated

a) Effects of surface temperature of the substrate, T_s = 22°C and 50°C

b) Varying manganese oxide particle concentration

c) Surface hydrophilicity vs surface hydrophobicity

d) Effects of surface tension of the suspending liquid: comparison of deionized water and deionized water/ethanol (90/10)

Chapter 2

Results and Discussion

2.1 Experimental Methods

The solutions of both MnO_2-water based and MnO_2-water-ethanol (90/10 vol%) based were prepared with mass concentration of MnO_2 of 0.5 and 0.75wt%. The solutions were stabilized by tip sonication for 30 minutes. All the samples were prepared just before the evaporation experiments.

Experiments were performed by employing a microscopy system to examine the drying process of droplets from top view. The brightfield function of the microscope was applied to examine the particle motion during evaporation and the formed deposited profile after the evaporation completed. The size of the droplets was $1\mu l \pm 0.1$.

2.2 Discussions

This section provides qualitative analysis from the evaporation of MnO_2 laden droplets on two substrates of different wettability (hydrophilic and hydrophobic) maintained at two temperatures (T_s= 22 and 50°C). First, the observations from 0.5wt% MnO_2-water based hydrophilic substrate are presented followed by that of 0.5wt% and 0.75wt% MnO_2-ethanol-water based.

Observations made through the optical microscope with sequential images are presented with explanations from existing literature.

2.2.1 Microscopic observations of Internal flow - 22°C hydrophilic substrate

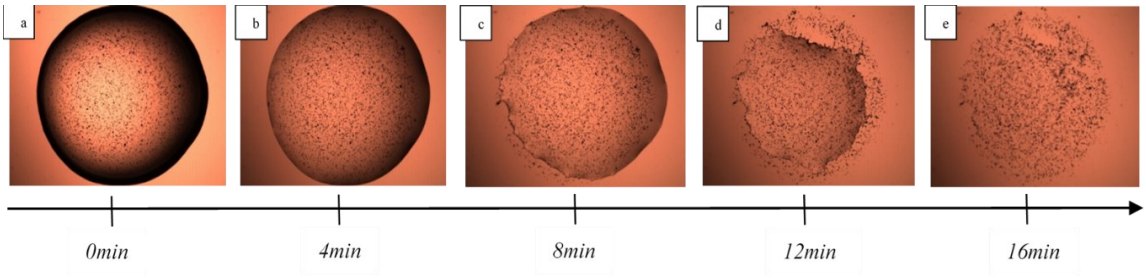

Figure 2-1: Drying sequence of MnO_2-water based sessile droplets (0.5wt%) on a nonheated hydrophilic substrate (at 22°C) *Scale bar is 254µm*

Optical microscopy was employed to observe the evaporation process of the particle laden droplets to understand the mechanism behind the deposition patterns. The microscope was focused on the initial triple line and the accumulation of particles were observed and followed as indicators of the flow.

At the beginning of evaporation, the chaotic flow of manganese oxide particles dragged toward the edge of the droplet by a radially outward capillary flow as showed the time images in Figure 2-1a, at the same time some of the particles remains at the liquid-vapor interface [25]. As evaporation proceeds, the flow profile changes and we observe a more uniform distribution of particles at the liquid-vapor interface while some particles deposited at the edge and move inward along the liquid-vapor interface generated from the weak thermal Marangoni flow [25],[112] (Figure 2- 1b-c) originating from the surface tension variation that is induced by the nonuniform evaporation at the three-phase line [113],[114].

Concurrently, the depinning of the contact line was observed and the particles deposited there begun to leave a trace on the substrate. Sangani et al. [115] reported that, the contact line tends to pin when the particle size is smaller and particle concentration is higher.

We speculate that the pinning of the contact line till midway through evaporation process was be due to some particles moving radially outwards towards the edge of the droplet which helped in pinning the contact line but the particles do not seem to have strong enough role in pinning the contact line, and thus the particles are dragged by the receding contact line [100].

As the contact line depins and move inwards it carried most of the particles (Figure 2-1d). In the final stages of evaporation those particles on top of the droplet surface deposit onto the substrate surface after complete evaporation and decrease in height of the droplet (Figure 2-1e). For the higher concentration of MnO_2 particles, we think the same mechanism of particle flow occurred which resulted in higher aggregation of particles between the periphery of the droplet and the interior of the pattern with a uniform pattern (Figure 2-3).

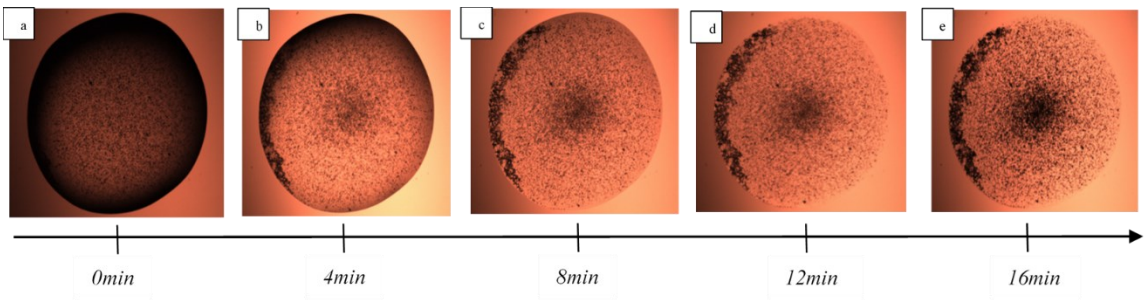

Figure 2-2: Figure 13: Drying sequence of MnO_2-water-ethanol based sessile droplets (0.5wt%) on a nonheated hydrophilic (at 22°C) *Scale bar is 254µm*

Even though we could not quantitively prove the added effect of ethanol and the mechanism of particle deposition in the evaporation droplet solely based deposited pattern,

the sequential evaporating images taken from the top view of the evaporating droplet gives some idea of the flow mechanism Figure 2-2(a) – (e).

Since we cannot measure the flowing in the droplet with particle image velocimetry now, we referred to the findings by Christy et al. [116] and Zhong and Duan [117] to explain the flow regimes within an evaporating droplet of water-based binary mixture suspended with nanoparticles. They classified three regimes in evaporation:

Regime I is chaotic flows are found to carry the particles to the liquid-vapor interface and to promote the formation of particle aggregation.

Regime II the vortices disappear, and the fluid flow slows down due to the inward Marangoni flow led by the nonuniform distribution of ethanol on the liquid−vapor interface.

Regime III is dominated by the evaporation of the water and the capillary flow driving particles radially outward is observed.

The patterns observed in MnO_2-water-ethanol based sessile droplet were influenced by the small change in ethanol and these combined flow regimes can result in the patterns we observed.

The flow pattern was observed based on the movement and aggregation of particles from the top view of the droplet. From the beginning of evaporation, rapid chaotic motion of nanoparticles was observed at the liquid-vapor interface with some aggregation particles (Figure 2-2a) [26]. After the chaotic flow, with time some particles reach the triple contact line and the particles at the liquid-vapor interfaces remained with further accumulation of the particles covering the central portion [26],[27],[117]. At this point we speculate that the more volatile components has evaporated [102],[104].

When the flow slowed down and the particles on the liquid-vapor interface begun to move to the center due to the Marangoni flow originating from the surface tension variation reported by Zhong and Duan [117] in regime II (Figure 2-2b) but at the same time we observed radial flow of particles towards the edge of the droplet with more aggregation towards the left side of the ring. The chaotic flow was observed to have ended by this point (4 minutes into the evaporation of the droplet).

By the half-life (8 minutes) of the droplet, more particles and some clustered particles deposited at the edge begun to move inwards while most remained at the edge (Figure 2-2c–d). This was observed till beyond (12 minutes) of the drying droplet (Figure 2-2d). Further accumulation and movement of particles to the center was observed till complete dry out with the deposited pattern (Figure 2-2e).

Zhong and Duan [27] observed that evaporating droplets with relatively low ethanol concentrations remain pinned throughout the evaporation process, a similar observation was reached in this study as can be seen in Figure 2-2(a) – (e). Further analysis made by them considered the changes in volume and contact angle. They found the reducing rate of the volume at the initial stage is more rapid than that at the late stage, and the contact angle the contact angle shows a faster reducing rate with a higher ethanol component.

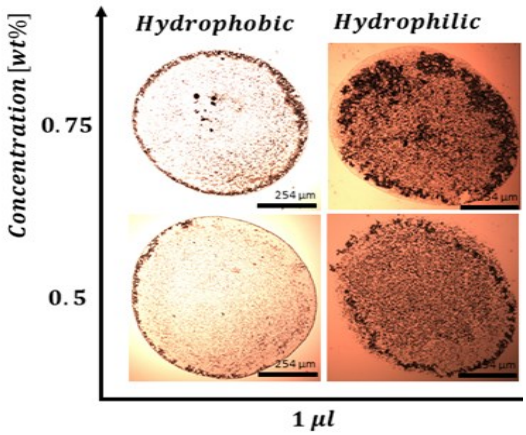

Figure 2-3: Images of deposited patterns after evaporation of MnO_2-water based droplets at 22°C for different particle concentrations on both hydrophilic and hydrophobic substrates

The patterns formed from the MnO_2-water based suspension shows relatively uniform distribution patterns on the hydrophobic surfaces on the contrary on the hydrophilic substrates most of the particles form clusters at the periphery and some detach from the outer ring (Figure 2-3).

Table 2-1: The list deposited patterns observed in Figure 2-3 (22°C on both hydrophilic and hydrophobic substrates)

Concentration [wt%]	$1\mu l$	
	Hydrophobic	Hydrophilic
0.5	Coffee-ring pattern Uniform Pattern	Uniform Pattern Coffee-ring pattern
0.75	Coffee-ring pattern Uniform Pattern	Uniform Pattern Coffee-ring pattern

2.2.2 Microscopic observations of Internal flow - 22°C hydrophobic substrate

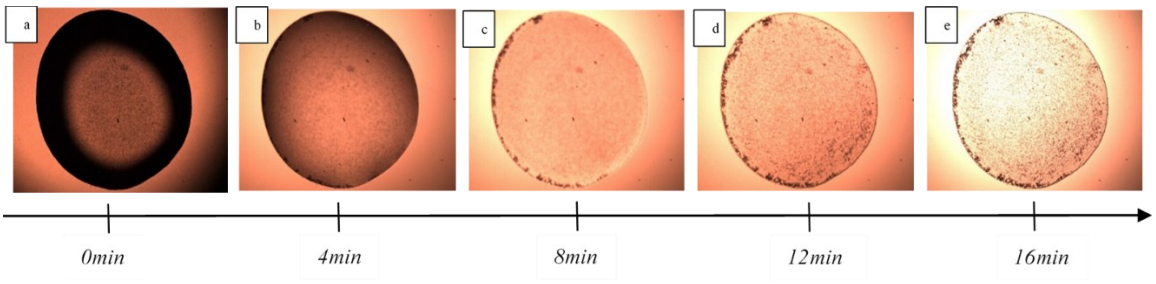

Figure 2-4: Drying sequence of MnO_2-water based sessile droplets (0.5wt%) on a nonheated hydrophobic substrate (at 22°C) *Scale bar is 254µm*

From the force balance or an energy minimization approach proposed by Orejon [43] the "depinning of the contact line will occur *only* when the Young unbalanced force at the contact line will be large enough to overcome the intrinsic energy barrier preventing the receding of the triple contact line" which is easier for hydrophobic substrate.

During the evaporation of MnO_2-water-based sessile droplet on the hydrophobic, contrary to the findings of Patil et al. [80] it was observed that the droplet remained pinned throughout the entire evaporation process.

Capillary flows drove manganese oxide particles to the triple contact line and inward Marangoni flow brought some particles to the surface of the droplet, the same time we observed accumulation of particles at the edge (Figure 2-4a-b) this helped in pinning the droplet.

By the half-life (Figure 2-4c) of the sessile droplet the outward capillary flow dominated and more cluster of particles begun to move to the edge of the droplet and during the final stages the particles deposited on the surface of the droplet descended onto the substrate after complete evaporation of the droplet (Figure 2-4d-e). The build-up of particles at the triple contact line helped and acted as defects hindering the receding movement of the triple contact line (TCL) [113],[118],[119].

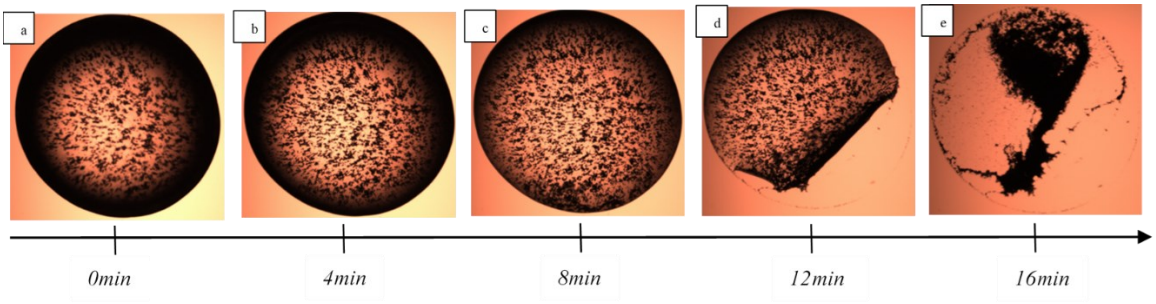

Figure 2-5: Drying sequence of MnO_2-water-ethanol based sessile droplets (0.75wt%) on a nonheated hydrophobic substrate (at 22°C) *Scale bar is 254µm*

When comparing our observations to those of Nguyen et al. [59], it must be pointed out that the transition through these modes were not observed in case MnO_2-water based droplets since the droplet was pinned through-out the evaporation process even though we believe further quantitative video analysis could prove otherwise due to the to limitations of the optical system. Nguyen et al. [59] that stated that three modes of evaporation of pure water droplet on a hydrophobic surface;

First stage the droplet is pinned and contact angle decreases (constant contact radius or CCR).

Second stage the droplet recedes/depins from the contact line and base radius decreases (constant contact angle or CCA), and

The final stage is mixed mode, where neither contact radius nor contact angle is constant. After contact angle reaches a critical value, the TCL starts receding and shrinking toward the droplet center.

For the MnO_2-water-ethanol droplets on the hydrophobic substrate, it appears the outward dominant flow resulted in the movement of particles towards the TCL and as evaporation progresses the accumulation of particles at the TCL increases (Figure 2-5a-c) till the half-life of the droplet. The accumulation of particles at the TCL we believe was responsible

for the pinning of the TCL until this stage owing to the increase in the concentration of the manganese oxide particles. As reported in literature the increase in concentration of particles has been found to prolong the pinning on the contact line during the first stage of evaporation and slows down the receding movement in the second stage on hydrophobic surfaces [59]. At the same time, we noticed that inward Marangoni flow of particles to the droplet surface.

About 12 minutes into evaporation we noticed the receding movement of the TCL which was captured (Figure 2-5d). At this point, we suspect that was the beginning of the "Stick-slip" behavior where the excess of droplet free energy must be high enough to overcome the energy barrier exerted by the particles and the substrate [34],[43] but this was not sustained. The increased concentration of particles here is presumed to be responsible for the pinning of the contact line till this point due to the increasing the local energy barriers. At this point (Figure 2-5c-d) we predict that the more volatile component has evaporated and the less volatile component is evaporating [102]. The fast evaporation of the ethanol in the first stage aided the rapid movement of particles towards the TCL.

In the final stage of the droplet lifetime (Figure 2-5e), the particles on the droplet top surface due to the Marangoni flows get deposited at the inner region with an thin outer ring.

It is worth mentioning that the outer ring formed in the case of 0.75 wt% MnO_2-water-ethanol hydrophobic (Figure 2-6) substrate is thicker than that of the 0.5 wt % confirming that the thickness of the rings form increases with the concentration [98].

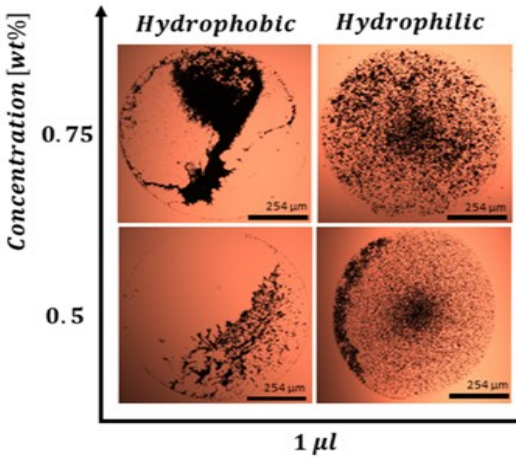

Figure 2-6: Images of deposited patterns after evaporation of MnO_2-water-ethanol based droplets at 22℃ for different particle concentrations on both hydrophilic and hydrophobic substrates

The patterns formed from the MnO_2-water-ethanol based suspension shows rings with inner deposits on the hydrophobic surfaces while on the hydrophilic substrates uniform deposition of patterns are formed with a higher amount of particles in the central portion of the ring (Figure 2-6).

Table 2-2: The list deposited patterns observed in Figure 2-7 (22℃ on both hydrophilic and hydrophobic substrates)

Concentration [wt%]	$1\mu l$	
	Hydrophobic	Hydrophilic
0.5	Ring-like pattern with inner deposit	Uniform Pattern
0.75	Ring-like pattern with inner deposit	Uniform Pattern

2.2.3 Deposited patterns observed on the heated substrate

It is important to note that the image contrast of the final deposited patterns recorded on the heated substrate is dependent on the thickness of the coffee ring structure or the patterns formed. Therefore, the region of the coffee ring structures appears to be darker as the number of the particle layers increases. Most of the patterns formed on the heated substrates were ring-like patterns with uniform distribution of particles.

Due to the fast evaporation rate of the droplets on a heated substrate, sequential images could not be captured during the process, only the final deposited patterns could be captured as shown in Figure 2-7 and Figure 2-8.

Marangoni flows, which is induced by a surface tension gradient, generated either by a composition (concentration gradient) or a temperature variation along the free surface plays a major role in the coffee ring formation [41],[120].

As reported extensively in literature, the influence of Marangoni velocity at high temperatures and the formation of the stagnation region near the contact line accounted for the deposited patterns observed at the end of evaporation [25]–[27],[80],[117]

Since the temperature gradient along the liquid−gas interface is larger for the heated substrate Marangoni flow brings more particles to the droplet apex point, and decreases the width as well as height of the deposited ring for hydrophilic [25]–[27],[80],[117].

These findings could be responsible for the final patterns observed in our studies in Figure 2-7 and Figure 2-8, but further studies need to be conducted to confirm this.

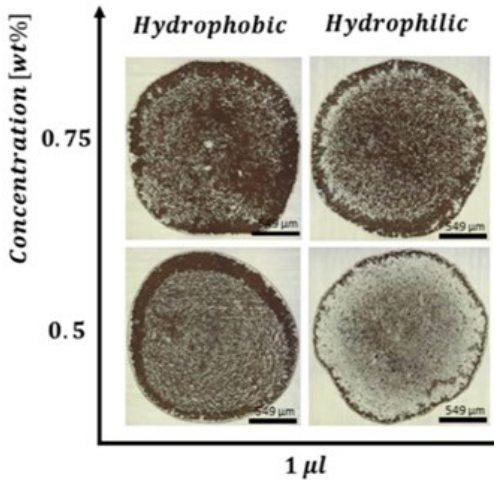

Figure 2-7: Images of deposited patterns after evaporation of MnO_2-water based droplets at 50℃ for different particle concentrations on both hydrophilic and hydrophobic substrates

The final deposited patterns at for MnO_2-water based droplets for both heated substrates showed coffee rings with a uniform distribution of particles (Figure 2-7). The accumulation of particles at the periphery of the droplet seems to be more at elevated temperatures

Table 2-3: The list deposited patterns observed in Figure 2-7 (50℃ on both hydrophilic and hydrophobic substrates)

Concentration [wt%]	$1\mu l$	
	Hydrophobic	Hydrophilic
0.5	Coffee-ring pattern Uniform Pattern	Uniform Pattern Dot-like pattern
0.75	Coffee-ring pattern Uniform Pattern	Uniform Pattern Dot-like pattern

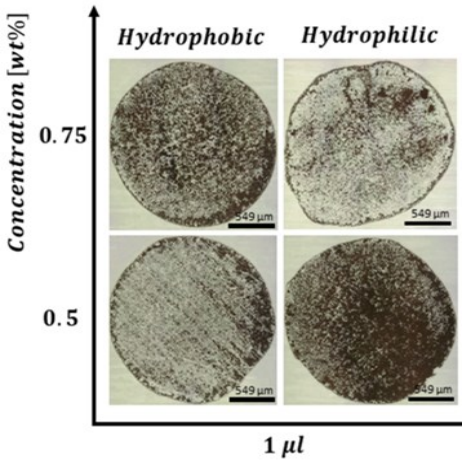

Figure 2-8: Images of deposited patterns after evaporation of MnO_2-water-ethanol based droplets at 50℃ for different particle concentrations on both hydrophilic and hydrophobic substrates.

The final deposited patterns for MnO_2-water-ethanol based droplets on the hydrophilic substrate the 0.5wt% MnO_2-water-ethanol droplet showed a uniformly distributed pattern with no ring, but the higher particle concentration showed a ring-like with uniformly distributed patterns. For both particle concentrations on hydrophobic substrates the final deposited patterns formed were ring-like patterns with uniformly distributed particles.

Table 2-4: The list deposited patterns observed in Figure 2-8 (50℃ on both hydrophilic and hydrophobic substrates)

Concentration [wt%]	$1\mu l$	
	Hydrophobic	Hydrophilic
0.5	Ring-like pattern Uniform Pattern	Uniform Pattern Dot-like pattern
0.75	Ring-like pattern Uniform Pattern	Uniform Pattern Ring-like pattern

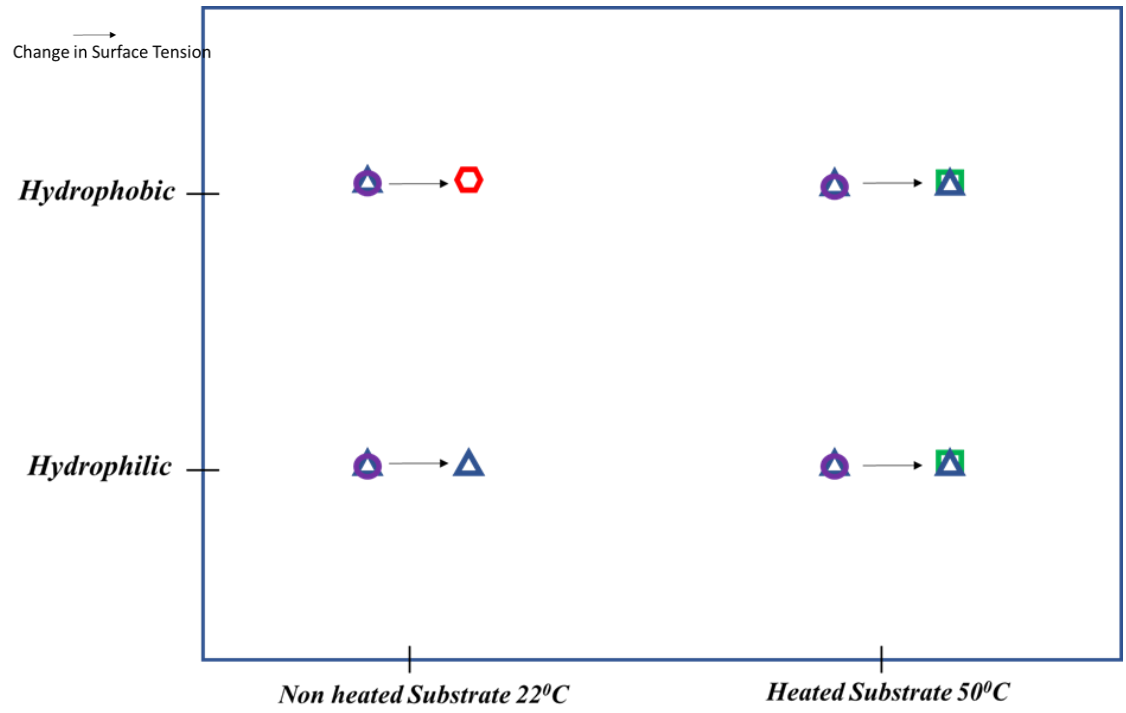

Figure 2-9: A plot of patterns vs process parameters

Coffee ring (0.5/0.75)wt%
Uniform pattern (0.5/0.75)wt%
Ring with inner deposits (0.5/0.75)wt%
Ring with uniform deposits (0.5/0.75)wt%

The plot above predicts the variation in patterns on nonheated and heated hydrophobic and hydrophilic substrates as a function of particle concentration and surface tension. The following conclusions could be drawn.

a) On nonheated substrates coffee-ring patterns with uniform depositions formed only uniform patterns when surface tension of the fluid changed – *Hydrophilic Substrate*

b) On nonheated substrates coffee-ring patterns with uniform depositions formed ring with inner deposits when surface tension of the fluid changed – *Hydrophobic Substrate*

c) On both nonheated and heated substrates coffee-ring patterns with uniform depositions formed ring with uniform when surface tension of the fluid changed – *Hydrophobic and Hydrophilic Substrate*

Chapter 3

3.1 Conclusion

The effects of substrate wettability, substrate temperature, surface tension and particle concentration of MnO_2 laden sessile droplets was investigated. On the nonheated substrates (hydrophobic and hydrophilic), the water-based sessile droplets formed coffee-rings with uniform distribution of particles at both low and high concentrations. This pattern was the same for the hydrophilic substrate (for 0.5wt% and 0.75wt%) with the addition of ethanol but a ring with inner deposit was formed on the hydrophobic substrate for both low and high concentrations. The patterns formed on the heated substrates (hydrophilic and hydrophobic) were ring-like patterns with uniform distribution of particles with the only difference being the variation in ring thickness.

This study provides a roadmap on the evaporation of manganese oxide particle laden droplets which can be used to model ink formulations to obtain desired patterns for applications such as inkjet printing of MnO_2 nanosheets for flexible electronic applications. The qualitative experimental data supports the hypothesis that these patterns are dependent on a variety of experimental conditions that has been extensively explored in literature for different types of particles.

Our results on manganese oxide laden particles are broadly consistent with most findings from literature.

Effects of surface temperature

Since the manganese oxide laden sessile droplets evaporated very quickly on the heated substrate, we could not observe the effects of substrate temperature during evaporation. Most of the assumptions made was based on the final deposited patterns reported in *Figures 2-7* and *Figures 2-8.* From these figures, non-isothermally heated substrates created different patterns from isothermally heated substrate [121].

Furthermore, they dominance of the thermal Marangoni flow at high temperatures could be responsible for the observed deposited patterns [25]–[27],[80],[117] but further analysis is needed to confirm these assumptions.

Effects of surface hydrophilicity and hydrophobicity

The effect of the substrate wettability on the final deposition patterns could be attributed to the pining and depinning behavior observed on both substrates. On hydrophobic substrates, the continuous receding of the contact line points out to a nonlinear evolution of either mass or volume in time [122],[123].

With equilibrium contact angle measurements, we should be able to differentiate the pinning behavior on both substrates. From our preliminary investigations, we observed a transition from CCR to CCA mode for the MnO_2-water-ethanol sessile droplet on the hydrophobic surface and the same for MnO_2-water based sessile droplet but future quantitative analysis has to be performed to explain this.

Effects of surface tension of the liquid

The effect of the addition of ethanol to our binary fluid was noticed by the fast evaporation and chaotic flow of particles that we observed at the initial stage of evaporation. We observed accumulation of particles and aggregate formation on the hydrophobic substrates during evaporation on the surface of the droplet. The accumulation and flow of particles to the surface of the droplets were observed on the hydrophilic substrates but without aggregation of particles.

The final deposited patterns observed on both substrates were different with the addition of ethanol and compared to the water-based ones.

Effects of particle concentration

The pining and depinning of the droplet were affected by the flow and accumulation of the particles at the contact line of the droplets. This was observed to be stronger in some cases than in others.

Also, the increase in particle concentration in both water-based and ethanol-water based manganese oxide sessile droplets prolonged the pinning of the contact line which we think was responsible for the formation of the coffee ring patterns. We also observed an increase in the size of rings and the number of particles deposited at the periphery in the final deposited patterns.

Despite the limitations of this studies these are valuable deductions in light of more detailed quantitative analysis that must be performed to correlate our preliminary investigation into the evaporation dynamics and flow mechanisms of particles in manganese oxide laden sessile droplets, we believe this study serves as a guide for further investigation.

3.2 Future Work

Droplet evaporation with particles remains a complex phenomenon, detailed understanding the underlying mechanisms of patterns as a result of particles laden droplets.

Future investigations are necessary to validate the kinds of conclusions that can be drawn from this study. Quantitative studies must be done to provide detailed understanding to our qualitative experimental observations. The visualization of colloidal particles during the evaporation process to understand the mechanism of deposition using a high-speed camera is recommended to correlate the observation made using the sequential timed images. Deposited patterns are influenced by the evaporation dynamics: for instance, in order to study the effect of substrate temperature, wettability, particle concentration and change in surface tension of the base fluid on colloidal droplets with particles, the temporal variation of the evolution of the droplet profiles such as volume, base diameter, contact angle, and height as a function of time can be analyzed through drop shape analyzer and analysis software. Using video editing/analysis to visually track the clusters of nanoparticles movement and measure a specific distance inside droplets with a proper calibration will help correlate the modes of evaporation on both substrates and understand the mechanisms responsible for the deposited patterns. Using the method of infrared thermography, the temporal temperature distribution of the liquid−gas and solid−gas interface could be recorded. This temperature measurement gives a better indication of the evaporation rate which can give a better indication of the Marangoni flows during the evaporation process which leads the variations in the patterns formed.

3.3 Societal Impact

The recent developments in inkjet printing of portable, wearable and flexible electronics have offered a lot of prospect for the growing micro electronics industry. Inkjet printing of conductive materials has been used in a wide range of applications, ranging from the manufacturing of display back panels, RF antenna, electronic packaging, solar cells and sensors.

The printed electronics market has been projected to rise by the 2025 of which inkjet printing plays a significant role [124]. For instance, printed displays are mostly used in consumer electronics such as wearables and mobile devices. The global demand for printed displays has resulted in increased demand for energy-efficient, thin, and flexible consumer electronic products. Also, leading manufacturers in the electronic industry have introduced thin, flexible, and energy-efficient displays developed using the organic light-emitting diodes (OLED) technology, which is mostly applied in printed electronics and is being used in high-end smartphones. Thin and rollable printed displays are used in a variety of consumer electronics. With significant strides being made in the field of flexible electronics and printed displays, these displays are expected to become the future mainstream displays for several consumer electronics.

Furthermore, for the application of complex ink formulations in injket printed electronics, the study of patterns formed post droplet evaporation of ink formulations, however, must consider the stability and reliability of the printing process with the new functional ink materials. Most of theses materials are abundant on earth and can be safely explored to advance the growing microelectronics industry.

For instance, conductive polymers have been widely used in gas sensors. These polymeric materials readily absorb gases into their interior causing a change in their electrical or electrochemical responses and these sensors are being applied in the industry and household. Transparent electrodes have been inkjet printed onto the surfaces of solar cells, which can be used to achieve greater energy conversion efficiencies.

With the growing energy demand now, the impact of finding stable ink formulations and its application in the energy generation and storage devices will be an important alternative for solving this problem.

In conclusion, advancements in inkjet-printed energy-storage devices especially on low-cost substrates will improve the global electronics industry and help in the manufacture of safe consumer products.

References

[1] Y. S. Yu, Z. Wang, and Y. P. Zhao, "Experimental and theoretical investigations of evaporation of sessile water droplet on hydrophobic surfaces," *J. Colloid Interface Sci.*, vol. 365, no. 1, pp. 254–259, 2012, doi: 10.1016/j.jcis.2011.09.007.

[2] S. Dash and S. V. Garimella, "Droplet evaporation dynamics on a superhydrophobic surface with negligible hysteresis," *Langmuir*, vol. 29, no. 34, pp. 10785–10795, 2013, doi: 10.1021/la402784c.

[3] A. K. Thokchom, Q. Zhou, D. J. Kim, D. Ha, and T. Kim, "Characterizing self-assembly and deposition behavior of nanoparticles in inkjet-printed evaporating droplets," *Sensors Actuators, B Chem.*, vol. 252, pp. 1063–1070, 2017, doi: 10.1016/j.snb.2017.06.045.

[4] H. Hu and R. G. Larson, "Evaporation of a sessile droplet on a substrate," *J. Phys. Chem. B*, vol. 106, no. 6, pp. 1334–1344, 2002, doi: 10.1021/jp0118322.

[5] F. Schönfeld, "Droplet Evaporation," in *Encyclopedia of Microfluidics and Nanofluidics*, D. Li, Ed. Boston, MA: Springer US, 2008, pp. 418–423.

[6] S. Y. Misyura, "Evaporation of a sessile water drop and a drop of aqueous salt solution," *Sci. Rep.*, vol. 7, no. 1, pp. 1–11, 2017, doi: 10.1038/s41598-017-15175-1.

[7] H. Hu and R. G. Larson, "Analysis of the microfluid flow in an evaporating sessile

droplet," *Langmuir*, vol. 21, no. 9, pp. 3963–3971, 2005, doi: 10.1021/la047528s.

[8] T. A. H. Nguyen, A. V. Nguyen, M. A. Hampton, Z. P. Xu, L. Huang, and V. Rudolph, "Theoretical and experimental analysis of droplet evaporation on solid surfaces," *Chem. Eng. Sci.*, vol. 69, no. 1, pp. 522–529, 2012, doi: 10.1016/j.ces.2011.11.009.

[9] Y. O. Popov, "Evaporative deposition patterns: Spatial dimensions of the deposit," *Phys. Rev. E - Stat. Nonlinear, Soft Matter Phys.*, vol. 71, no. 3, pp. 1–17, 2005, doi: 10.1103/PhysRevE.71.036313.

[10] S. A. Kulinich and M. Farzaneh, "Effect of contact angle hysteresis on water droplet evaporation from super-hydrophobic surfaces," *Appl. Surf. Sci.*, vol. 255, no. 7, pp. 4056–4060, 2009, doi: 10.1016/j.apsusc.2008.10.109.

[11] G. Guéna, C. Poulard, M. Voué, J. De Coninck, and A. M. Cazabat, "Evaporation of sessile liquid droplets," *Colloids Surfaces A Physicochem. Eng. Asp.*, vol. 291, no. 1–3, pp. 191–196, 2006, doi: 10.1016/j.colsurfa.2006.07.021.

[12] X. Fang, M. Pimentel, J. Sokolov, and M. Rafailovich, "Dewetting of the three-phase contact line on solids," *Langmuir*, vol. 26, no. 11. pp. 7682–7685, 2010, doi: 10.1021/la101249k.

[13] N. M. Kovalchuk, A. Trybala, and V. M. Starov, "Evaporation of sessile droplets," *Curr. Opin. Colloid Interface Sci.*, vol. 19, no. 4, pp. 336–342, 2014, doi: 10.1016/j.cocis.2014.07.005.

[14] R. D. Deegan, O. Bakajin, T. F. Dupont, G. Huber, S. R. Nagel, and T. A. Witten, "Capillary flow as the cause of ring stains from dried liquid drops," *Nature*, vol. 389, no. 6653, pp. 827–829, 1997, doi: 10.1038/39827.

[15] H. Hu and R. G. Larson, “Analysis of the effects of marangoni stresses on the microflow in an evaporating sessile droplet,” *Langmuir*, vol. 21, no. 9, pp. 3972–3980, 2005, doi: 10.1021/la0475270.

[16] H. Hu and R. G. Larson, “Marangoni effect reverses coffee-ring depositions,” *J. Phys. Chem. B*, vol. 110, no. 14, pp. 7090–7094, 2006, doi: 10.1021/jp0609232.

[17] T. Still, P. J. Yunker, and A. G. Yodh, “Surfactant-induced Marangoni eddies alter the coffee-rings of evaporating colloidal drops,” *Langmuir*, vol. 28, no. 11, pp. 4984–4988, 2012, doi: 10.1021/la204928m.

[18] A. Crivoi and F. Duan, “Effect of surfactant on the drying patterns of graphite nanofluid droplets,” *J. Phys. Chem. B*, vol. 117, no. 19, pp. 5932–5938, 2013, doi: 10.1021/jp401751z.

[19] X. Zhong, C. Wu, and F. Duan, “From enhancement to elimination of dual-ring pattern of nanoparticles from sessile droplets by heating the substrate,” *Appl. Therm. Eng.*, vol. 115, pp. 1418–1423, 2017, doi: 10.1016/j.applthermaleng.2016.11.002.

[20] S. Tarafdar, Y. Y. Tarasevich, M. Dutta Choudhury, T. Dutta, and D. Zang, “Droplet Drying Patterns on Solid Substrates: From Hydrophilic to Superhydrophobic Contact to Levitating Drops,” *Adv. Condens. Matter Phys.*, vol. 2018, no. February, 2018, doi: 10.1155/2018/5214924.

[21] A. Askounis, K. Sefiane, V. Koutsos, and M. E. R. Shanahan, “The effect of evaporation kinetics on nanoparticle structuring within contact line deposits of volatile drops,” *Colloids Surfaces A Physicochem. Eng. Asp.*, vol. 441, pp. 855–866, 2014, doi: 10.1016/j.colsurfa.2012.10.017.

[22] R. Bhardwaj, X. Fang, P. Somasundaran, and D. Attinger, “Self-assembly of colloidal particles from evaporating droplets: Role of DLVO interactions and proposition of a phase diagram,” *Langmuir*, vol. 26, no. 11, pp. 7833–7842, 2010, doi: 10.1021/la9047227.

[23] P. J. Yunker, T. Still, M. A. Lohr, and A. G. Yodh, “Suppression of the coffee-ring effect by shape-dependent capillary interactions,” *Nature*, vol. 476, no. 7360, pp. 308–311, 2011, doi: 10.1038/nature10344.

[24] N. D. Patil, P. G. Bange, R. Bhardwaj, and A. Sharma, “E ff ects of Substrate Heating and Wettability on Evaporation Dynamics and Deposition Patterns for a Sessile Water Droplet Containing Colloidal Particles,” 2016, doi: 10.1021/acs.langmuir.6b02769.

[25] M. Parsa, S. Harmand, K. Sefiane, M. Bigerelle, and R. Deltombe, “Effect of substrate temperature on pattern formation of nanoparticles from volatile drops,” *Langmuir*, vol. 31, no. 11. pp. 3354–3367, 2015, doi: 10.1021/acs.langmuir.5b00362.

[26] M. Parsa, R. Boubaker, S. Harmand, K. Sefiane, M. Bigerelle, and R. Deltombe, “Patterns from dried water-butanol binary-based nanofluid drops,” *J. Nanoparticle Res.*, vol. 19, no. 8, 2017, doi: 10.1007/s11051-017-3951-2.

[27] X. Zhong and F. Duan, “Evaporation of sessile droplets affected by graphite nanoparticles and binary base fluids,” *J. Phys. Chem. B*, vol. 118, no. 47, pp. 13636–13645, 2014, doi: 10.1021/jp508051y.

[28] R. G. Picknett and R. Bexon, “The evaporation of sessile or pendant drops in still air,” *J. Colloid Interface Sci.*, vol. 61, no. 2, pp. 336–350, 1977, doi:

10.1016/0021-9797(77)90396-4.

[29] M. R. Gunjan and R. Raj, “Dynamic Roughness Ratio-Based Framework for Modeling Mixed Mode of Droplet Evaporation,” *Langmuir*, vol. 33, no. 28. pp. 7191–7201, 2017, doi: 10.1021/acs.langmuir.7b01653.

[30] M. Gao, P. Kong, L. X. Zhang, and J. N. Liu, “An experimental investigation of sessile droplets evaporation on hydrophilic and hydrophobic heating surface with constant heat flux,” *Int. Commun. Heat Mass Transf.*, vol. 88, pp. 262–268, 2017, doi: 10.1016/j.icheatmasstransfer.2017.09.010.

[31] X. Zhang *et al.*, “Mixed mode of dissolving immersed nanodroplets at a solid-water interface,” *Soft Matter*, vol. 11, no. 10, pp. 1889–1900, 2015, doi: 10.1039/c4sm02397h.

[32] A. K. Panwar, S. K. Barthwal, and S. Ray, “Effect of evaporation on the contact angle of a sessile drop on solid substrates,” *J. Adhes. Sci. Technol.*, vol. 17, no. 10, pp. 1321–1329, 2003, doi: 10.1163/156856103769172760.

[33] C. Bourgès-Monnier and M. E. R. Shanahan, “Influence of Evaporation on Contact Angle,” *Langmuir*, vol. 11, no. 7, pp. 2820–2829, 1995, doi: 10.1021/la00007a076.

[34] M. E. R. Shanahan, “Simple Theory of ‘Stick-Slip’ Wetting Hysteresis,” *Langmuir*, vol. 11, no. 3, pp. 1041–1043, 1995, doi: 10.1021/la00003a057.

[35] A. Askounis, “Surface nano-patterning using the coffee-stain effect,” p. 163, 2014.

[36] D. Orejon, K. Sefiane, and M. E. R. Shanahan, “Stick-slip of evaporating droplets: Substrate hydrophobicity and nanoparticle concentration,” *Langmuir*, vol. 27, no.

21, pp. 12834–12843, 2011, doi: 10.1021/la2026736.

[37] K. Uno, K. Hayashi, T. Hayashi, K. Ito, and H. Kitano, "Particle adsorption in evaporating droplets of polymer latex dispersions on hydrophilic and hydrophobic surfaces," *Colloid and Polymer Science*, vol. 276, no. 9. pp. 810–815, 1998, doi: 10.1007/s003960050314.

[38] M. Majumder *et al.*, "Overcoming the 'coffee-stain' effect by compositional marangoni-flow-assisted drop-drying," *J. Phys. Chem. B*, vol. 116, no. 22, pp. 6536–6542, 2012, doi: 10.1021/jp3009628.

[39] X. Shen, C. M. Ho, and T. S. Wong, "Minimal size of coffee ring structure," *J. Phys. Chem. B*, vol. 114, no. 16, pp. 5269–5274, 2010, doi: 10.1021/jp912190v.

[40] J. Park and J. Moon, "Control of colloidal particle deposit patterns within picoliter droplets ejected by ink-jet printing," *Langmuir*, vol. 22, no. 8, pp. 3506–3513, 2006, doi: 10.1021/la053450j.

[41] H. Kim, F. Boulogne, E. Um, I. Jacobi, E. Button, and H. A. Stone, "Controlled Uniform Coating from the Interplay of Marangoni Flows and Surface-Adsorbed Macromolecules," *Phys. Rev. Lett.*, vol. 116, no. 12, pp. 1–5, 2016, doi: 10.1103/PhysRevLett.116.124501.

[42] C. Seo, D. Jang, J. Chae, and S. Shin, "Altering the coffee-ring effect by adding a surfactant-like viscous polymer solution," *Sci. Rep.*, vol. 7, no. 1, pp. 1–9, 2017, doi: 10.1038/s41598-017-00497-x.

[43] D. Orejon, "A Study of Nanosuspension Droplets Free Evaporation and Electrowetting By," no. November 2013, 2013.

[44] K. Sefiane, "On the role of structural disjoining pressure and contact line pinning

in critical heat flux enhancement during boiling of nanofluids," *Appl. Phys. Lett.*, vol. 89, no. 4, pp. 1–4, 2006, doi: 10.1063/1.2222283.

[45] M. Anyfantakis and D. Baigl, "Manipulating the Coffee-Ring Effect: Interactions at Work," *ChemPhysChem*, vol. 16, no. 13, pp. 2726–2734, 2015, doi: 10.1002/cphc.201500410.

[46] Y. Li, Q. Yang, M. Li, and Y. Song, "Rate-dependent interface capture beyond the coffee-ring effect," *Sci. Rep.*, vol. 6, no. March, pp. 1–8, 2016, doi: 10.1038/srep24628.

[47] T. P. Bigioni, X. M. Lin, T. T. Nguyen, E. I. Corwin, T. A. Witten, and H. M. Jaeger, "Kinetically driven self assembly of highly ordered nanoparticle monolayers," *Nat. Mater.*, vol. 5, no. 4, pp. 265–270, 2006, doi: 10.1038/nmat1611.

[48] J. Y. Kim, K. Cho, S. A. Ryu, S. Y. Kim, and B. M. Weon, "Crack formation and prevention in colloidal drops," *Sci. Rep.*, vol. 5, pp. 1–9, 2015, doi: 10.1038/srep13166.

[49] L. Pauchard, F. Parisse, and C. Allain, "Influence of salt content on crack patterns formed through colloidal suspension desiccation," *Phys. Rev. E*, vol. 59, no. 3, pp. 3737–3740, Mar. 1999, doi: 10.1103/PhysRevE.59.3737.

[50] H. M. Gorr, J. M. Zueger, D. R. McAdams, and J. A. Barnard, "Salt-induced pattern formation in evaporating droplets of lysozyme solutions," *Colloids Surfaces B Biointerfaces*, vol. 103, pp. 59–66, 2013, doi: 10.1016/j.colsurfb.2012.09.043.

[51] Y. Zhang, Y. Qian, Z. Liu, Z. Li, and D. Zang, "Surface wrinkling and cracking

dynamics in the drying of colloidal droplets," *Eur. Phys. J. E*, vol. 37, no. 9, pp. 1–7, 2014, doi: 10.1140/epje/i2014-14084-3.

[52] J. R. Moffat, K. Sefiane, and M. E. R. Shanahan, "Effect of TiO2 nanoparticles on contact line stick-slip behavior of volatile drops," *J. Phys. Chem. B*, vol. 113, no. 26, pp. 8860–8866, 2009, doi: 10.1021/jp902062z.

[53] T. Dutta, A. Giri, M. D. Choudhury, and S. Tarafdar, "Experiment and simulation of multifractal growth of crystalline NaCl aggregates in aqueous gelatin medium," *Colloids Surfaces A Physicochem. Eng. Asp.*, vol. 432, pp. 127–131, 2013, doi: 10.1016/j.colsurfa.2013.04.040.

[54] G. Chen and G. J. Mohamed, "Complex protein patterns formation via salt-induced self-assembly and droplet evaporation," *Eur. Phys. J. E*, vol. 33, no. 1, pp. 19–26, 2010, doi: 10.1140/epje/i2010-10649-4.

[55] D. Kaya, V. A. Belyi, and M. Muthukumar, "Pattern formation in drying droplets of polyelectrolyte and salt," *J. Chem. Phys.*, vol. 133, no. 11, 2010, doi: 10.1063/1.3493687.

[56] N. Shahidzadeh-Bonn, S. Rafai, D. Bonn, and G. Wegdam, "Salt crystallization during evaporation: Impact of interfacial properties," *Langmuir*, vol. 24, no. 16, pp. 8599–8605, 2008, doi: 10.1021/la8005629.

[57] T. A. Yakhno *et al.*, "The informative-capacity phenomenon of drying drops," *IEEE Eng. Med. Biol. Mag.*, vol. 24, no. 2, pp. 96–104, 2005, doi: 10.1109/MEMB.2005.1411354.

[58] X. Zhong, J. Ren, and F. Duan, "Wettability Effect on Evaporation Dynamics and Crystalline Patterns of Sessile Saline Droplets," *J. Phys. Chem. B*, vol. 121, no.

33, pp. 7924–7933, 2017, doi: 10.1021/acs.jpcb.7b03690.

[59] T. A. H. Nguyen, M. A. Hampton, and A. V. Nguyen, “Evaporation of nanoparticle droplets on smooth hydrophobic surfaces: The inner coffee ring deposits,” *J. Phys. Chem. C*, vol. 117, no. 9, pp. 4707–4716, 2013, doi: 10.1021/jp3126939.

[60] A. Crivoi and F. Duan, “Fingering structures inside the coffee-ring pattern,” *Colloids Surfaces A Physicochem. Eng. Asp.*, vol. 432, pp. 119–126, 2013, doi: 10.1016/j.colsurfa.2013.04.051.

[61] Y. F. Li, Y. J. Sheng, and H. K. Tsao, “Evaporation stains: Suppressing the coffee-ring effect by contact angle hysteresis,” *Langmuir*, vol. 29, no. 25, pp. 7802–7811, 2013, doi: 10.1021/la400948e.

[62] S. G. Sanfélix, “Manganese Oxide Nanoparticles : Synthesis and Magnetic Properties Erasmus Exchange,” no. Marburg 07-08, p. 91, 2016.

[63] J. Z. Zhang, “Synthesis and Fabrication of Nanomaterials,” *Opt. Prop. Spectrosc. Nanomater.*, no. January 2015, pp. 77–115, 2009, doi: 10.1142/9789812836663_0004.

[64] C. Properties and P. Properties, “Manganese Oxide (Mn2O3) Nanoparticles - Properties , Applications,” pp. 2–3, 2013.

[65] “Mangnese.pdf.” .

[66] L. Della Puppa, M. Komárek, F. Bordas, J. C. Bollinger, and E. Joussein, “Adsorption of copper, cadmium, lead and zinc onto a synthetic manganese oxide,” *J. Colloid Interface Sci.*, vol. 399, pp. 99–106, 2013, doi: 10.1016/j.jcis.2013.02.029.

[67] X. H. Feng, L. M. Zhai, W. F. Tan, F. Liu, and J. Z. He, “Adsorption and redox reactions of heavy metals on synthesized Mn oxide minerals,” *Environ. Pollut.*, vol. 147, no. 2, pp. 366–373, 2007, doi: 10.1016/j.envpol.2006.05.028.

[68] “A review on the synthesis of SiC from plant ba.pdf.” .

[69] T. Soejima, K. Nishizawa, and R. Isoda, “Monodisperse manganese oxide nanoparticles: Synthesis, characterization, and chemical reactivity,” *J. Colloid Interface Sci.*, vol. 510, pp. 272–279, 2018, doi: 10.1016/j.jcis.2017.09.082.

[70] C. W. Chew Ling, “Synthesis and Characterization of Manganese Dioxide Nanoparticles and Thin Films.” p. 24, 2007.

[71] M. H. Tavakoli Dastjerdi, G. Habibagahi, A. Ghahramani, A. Karimi-Jashni, and S. Zeinali, “Removal of dissolved toluene in underground water with nanowires of manganese oxide,” *Adsorpt. Sci. Technol.*, vol. 36, no. 1–2, pp. 393–407, 2018, doi: 10.1177/0263617417698469.

[72] J. E. ten Elshof and Y. Wang, “Advances in Ink-Jet Printing of MnO2-Nanosheet Based Pseudocapacitors,” *Small Methods*, vol. 3, no. 8, pp. 1–12, 2019, doi: 10.1002/smtd.201800318.

[73] Z. Fan, Z. Zhou, W. Zhang, X. Zhang, and J. M. Lin, “Inkjet printing based ultra-small MnO2 nanosheets synthesis for glutathione sensing,” *Talanta*, vol. 225, no. September 2020, p. 121989, 2021, doi: 10.1016/j.talanta.2020.121989.

[74] Y. Wang, Y. Z. Zhang, D. Dubbink, and J. E. ten Elshof, “Inkjet printing of δ-MnO2 nanosheets for flexible solid-state micro-supercapacitor,” *Nano Energy*, vol. 49, no. May, pp. 481–488, 2018, doi: 10.1016/j.nanoen.2018.05.002.

[75] A. G. Kelly *et al.*, “All-printed thin-film transistors from networks of liquid-

exfoliated nanosheets," *Science (80-.).*, vol. 356, no. 6333, pp. 69–73, 2017, doi: 10.1126/science.aal4062.

[76] F. Torrisi *et al.*, "Inkjet-printed graphene electronics," *ACS Nano*, vol. 6, no. 4, pp. 2992–3006, 2012, doi: 10.1021/nn2044609.

[77] X. Peng *et al.*, "Perovskite and Organic Solar Cells Fabricated by Inkjet Printing: Progress and Prospects," *Adv. Funct. Mater.*, vol. 27, no. 41, 2017, doi: 10.1002/adfm.201703704.

[78] X. Chang *et al.*, "Carbon-Based CsPbBr3 Perovskite Solar Cells: All-Ambient Processes and High Thermal Stability," *ACS Appl. Mater. Interfaces*, vol. 8, no. 49, pp. 33649–33655, 2016, doi: 10.1021/acsami.6b11393.

[79] H. C. Chan, S. Paik, J. B. Tipton, and K. D. Kihm, "Effect of nanoparticle sizes and number densities on the evaporation and dryout characteristics for strongly pinned nanofluid droplets," *Langmuir*, vol. 23, no. 6, pp. 2953–2960, 2007, doi: 10.1021/la061661y.

[80] N. D. Patil, P. G. Bange, R. Bhardwaj, and A. Sharma, "Effects of Substrate Heating and Wettability on Evaporation Dynamics and Deposition Patterns for a Sessile Water Droplet Containing Colloidal Particles," *Langmuir*, vol. 32, no. 45, pp. 11958–11972, 2016, doi: 10.1021/acs.langmuir.6b02769.

[81] Y. Li, C. Lv, Z. Li, D. Quéré, and Q. Zheng, "From coffee rings to coffee eyes," *Soft Matter*, vol. 11, no. 23, p. 4669—4673, Jun. 2015, doi: 10.1039/c5sm00654f.

[82] K. S. Birdi, D. T. Vu, and A. Winter, "A study of the evaporation rates of small water drops placed on a solid surface," *J. Phys. Chem.*, vol. 93, no. 9, pp. 3702–3703, 1989, doi: 10.1021/j100346a065.

[83] G. Mchale, S. M. Rowan, M. I. Newton, and M. K. Banerjee, “Evaporation and the Wetting of a Low-Energy Solid Surface,” vol. 5647, no. 97, pp. 1964–1967, 1998.

[84] C. National, D. Recherche, M. P. M. Fourt, E. Nationale, M. De Paris, and E. Cedex, “Influence of Evaporation,” vol. 7, no. 8, pp. 485–493, 1995.

[85] E. Widjaja and M. T. Harris, “Particle Deposition Study During Sessile Drop Evaporation,” vol. 54, no. 9, 2008, doi: 10.1002/aic.

[86] D. M. Andersona and S. H. Davis, “The spreading of volatile liquid droplets on heated surfaces,” vol. 7, no. 2, 1995.

[87] M. E. R. Shanahan, K. Sefiane, and J. R. Moffat, “Dependence of volatile droplet lifetime on the hydrophobicity of the substrate,” *Langmuir*, vol. 27, no. 8, pp. 4572–4577, 2011, doi: 10.1021/la200437s.

[88] V. Recei, V. No, V. Re, M. Recei, and V. December, “Pinning, Retraction, and Terracing of Evaporating Droplets Containing Nanoparticles,” no. 22, pp. 3601–3609, 2009.

[89] J. Lee, P. Khac, S. Chan, and H. Chung, “Talanta Development of hydrophobic surface substrates enabling reproducible drop-and-dry spectroscopic measurements,” *Talanta*, vol. 153, pp. 31–37, 2016, doi: 10.1016/j.talanta.2016.02.053.

[90] V. H. Chhasatia and Y. Sun, “Interaction of bi-dispersed particles with contact line in an evaporating colloidal drop,” *Soft Matter*, vol. 7, no. 21, pp. 10135–10143, 2011, doi: 10.1039/c1sm06393f.

[91] S. Chatterjee, M. Kumar, J. S. Murallidharan, and R. Bhardwaj, “Evaporation of

Initially Heated Sessile Droplets and the Resultant Dried Colloidal Deposits on Substrates Held at Ambient Temperature," *Langmuir*, vol. 36, no. 29, pp. 8407–8421, 2020, doi: 10.1021/acs.langmuir.0c00756.

[92] E. Xu, J. Luo, and D. Guo, "Criterion for reversal of thermal marangoni flow in drying drops," *Langmuir*, vol. 26, no. 3, pp. 1918–1922, 2010, doi: 10.1021/la902666r.

[93] X. Zhong and F. Duan, "Disk to dual ring deposition transformation in evaporating nanofluid droplets from substrate cooling to heating," *Phys. Chem. Chem. Phys.*, vol. 18, no. 30, pp. 20664–20671, 2016, doi: 10.1039/c6cp03231a.

[94] M. Anyfantakis, D. Baigl, and B. P. Binks, "Evaporation of Drops Containing Silica Nanoparticles of Varying Hydrophobicities: Exploiting Particle-Particle Interactions for Additive-Free Tunable Deposit Morphology," *Langmuir*, vol. 33, no. 20, pp. 5025–5036, 2017, doi: 10.1021/acs.langmuir.7b00807.

[95] G. Karapetsas, K. C. Sahu, and O. K. Matar, "Evaporation of Sessile Droplets Laden with Particles and Insoluble Surfactants," *Langmuir*, vol. 32, no. 27, pp. 6871–6881, 2016, doi: 10.1021/acs.langmuir.6b01042.

[96] J. R. Moffat, K. Sefiane, and M. E. R. Shanahan, "Nanofluid Droplet Evaporation Kinetics and Wetting Dynamics on Flat Substrates," *J. Nano Res.*, vol. 7, pp. 75–80, 2009, doi: 10.4028/www.scientific.net/JNanoR.7.75.

[97] D. Brutin, "Influence of relative humidity and nano-particle concentration on pattern formation and evaporation rate of pinned drying drops of nanofluids," *Colloids Surfaces A Physicochem. Eng. Asp.*, vol. 429, pp. 112–120, 2013, doi: 10.1016/j.colsurfa.2013.03.012.

[98] K. Sefiane, “On the formation of regular patterns from drying droplets and their potential use for bio-medical applications,” *J. Bionic Eng.*, vol. 7, no. SUPPL., pp. S82–S93, 2010, doi: 10.1016/S1672-6529(09)60221-3.

[99] H. H. Lee, S. C. Fu, C. Y. Tso, and C. Y. H. Chao, “Study of residue patterns of aqueous nanofluid droplets with different particle sizes and concentrations on different substrates,” *Int. J. Heat Mass Transf.*, vol. 105, pp. 230–236, 2017, doi: 10.1016/j.ijheatmasstransfer.2016.09.093.

[100] Y. Choi, J. Han, and C. Kim, “Pattern formation in drying of particle-laden sessile drops of polymer solutions on solid substrates,” *Korean J. Chem. Eng.*, vol. 28, no. 11, pp. 2130–2136, 2011, doi: 10.1007/s11814-011-0084-7.

[101] E. L. Talbot, A. Berson, and C. D. Bain, “Drying and deposition of picolitre droplets of colloidal suspensions in binary solvent mixtures,” *Int. Conf. Digit. Print. Technol.*, no. June, pp. 420–423, 2012.

[102] K. Sefiane, L. Tadrist, and M. Douglas, “Experimental study of evaporating water-ethanol mixture sessile drop: Influence of concentration,” *Int. J. Heat Mass Transf.*, vol. 46, no. 23, pp. 4527–4534, 2003, doi: 10.1016/S0017-9310(03)00267-9.

[103] A. K. H. Cheng, D. M. Soolaman, and H. Z. Yu, “Evaporation of microdroplets of ethanol-water mixtures on gold surfaces modified with self-assembled monolayers,” *J. Phys. Chem. B*, vol. 110, no. 23, pp. 11267–11271, 2006, doi: 10.1021/jp0572885.

[104] C. Liu, E. Bonaccurso, and H. J. Butt, “Evaporation of sessile water/ethanol drops in a controlled environment,” *Phys. Chem. Chem. Phys.*, vol. 10, no. 47, pp. 7150–

7157, 2008, doi: 10.1039/b808258h.

[105] L. Y. Barash, T. P. Bigioni, V. M. Vinokur, and L. N. Shchur, “Evaporation and fluid dynamics of a sessile drop of capillary size,” *Phys. Rev. E - Stat. Nonlinear, Soft Matter Phys.*, vol. 79, no. 4, pp. 1–16, 2009, doi: 10.1103/PhysRevE.79.046301.

[106] L. Y. Barash, “Dependence of fluid flows in an evaporating sessile droplet on the characteristics of the substrate,” *Int. J. Heat Mass Transf.*, vol. 84, no. October, pp. 419–426, 2015, doi: 10.1016/j.ijheatmasstransfer.2015.01.014.

[107] Y. H. Chen, W. N. Hu, J. Wang, F. J. Hong, and P. Cheng, “Transient effects and mass convection in sessile droplet evaporation: The role of liquid and substrate thermophysical properties,” *Int. J. Heat Mass Transf.*, vol. 108, pp. 2072–2087, 2017, doi: 10.1016/j.ijheatmasstransfer.2017.01.050.

[108] Z. Qiao, Z. Wang, C. Zhang, S. Yuan, Y. Zhu, and J. Wang, “PVAm–PIP/PS composite membrane with high performance for CO_2/N_2 separation,” *AIChE J.*, vol. 59, no. 4, pp. 215–228, 2012, doi: 10.1002/aic.

[109] L. Wang, Z. Liu, X. Wang, and Y. Yan, “Investigation on the droplet evaporation process on local heated substrates with different wettability,” *Heat Mass Transf. und Stoffuebertragung*, 2020, doi: 10.1007/s00231-020-03005-6.

[110] W. D. Ristenpart, P. G. Kim, C. Domingues, J. Wan, and H. A. Stone, “Influence of substrate conductivity on circulation reversal in evaporating drops,” *Phys. Rev. Lett.*, vol. 99, no. 23, pp. 1–4, 2007, doi: 10.1103/PhysRevLett.99.234502.

[111] R. Chen, L. Zhang, D. Zang, and W. Shen, “Wetting and Drying of Colloidal Droplets: Physics and Pattern Formation,” *Adv. Colloid Sci.*, no. November, 2016,

doi: 10.5772/65301.

[112] X. Xu and J. Luo, “Marangoni flow in an evaporating water droplet,” *Appl. Phys. Lett.*, vol. 91, no. 12, pp. 19–22, 2007, doi: 10.1063/1.2789402.

[113] R. D. Deegan, “Pattern formation in drying drops,” *Phys. Rev. E - Stat. Physics, Plasmas, Fluids, Relat. Interdiscip. Top.*, vol. 61, no. 1, pp. 475–485, 2000, doi: 10.1103/PhysRevE.61.475.

[114] F. Duan and C. A. Ward, “Investigation of local evaporation flux and vapor-phase pressure at an evaporative droplet interface,” *Langmuir*, vol. 25, no. 13, pp. 7424–7431, 2009, doi: 10.1021/la900337j.

[115] A. S. Sangani, C. Lu, K. Su, and J. A. Schwarz, “Capillary force on particles near a drop edge resting on a substrate and a criterion for contact line pinning,” *Phys. Rev. E*, vol. 80, no. 1, p. 11603, Jul. 2009, doi: 10.1103/PhysRevE.80.011603.

[116] J. R. E. Christy, Y. Hamamoto, and K. Sefiane, “Flow transition within an evaporating binary mixture sessile drop,” *Phys. Rev. Lett.*, vol. 106, no. 20, pp. 1–4, 2011, doi: 10.1103/PhysRevLett.106.205701.

[117] X. Zhong and F. Duan, “Flow regime and deposition pattern of evaporating binary mixture droplet suspended with particles,” *Eur. Phys. J. E*, vol. 39, no. 2, pp. 1–6, 2016, doi: 10.1140/epje/i2016-16018-5.

[118] R. D. Deegan, O. Bakajin, T. F. Dupont, G. Huber, S. R. Nagel, and T. A. Witten, “Contact line deposits in an evaporating drop,” *Phys. Rev. E - Stat. Physics, Plasmas, Fluids, Relat. Interdiscip. Top.*, vol. 62, no. 1 B, pp. 756–765, 2000, doi: 10.1103/PhysRevE.62.756.

[119] G. R. Duursma, K. Sefiane, and S. David, “Advancing and receding contact lines

on patterned structured surfaces," *Chem. Eng. Res. Des.*, vol. 88, no. 5–6, pp. 737–743, 2010, doi: 10.1016/j.cherd.2009.10.004.

[120] L. Y. Barash, "Marangoni convection in an evaporating droplet: Analytical and numerical descriptions," *Int. J. Heat Mass Transf.*, vol. 102, no. June 2016, pp. 445–454, 2016, doi: 10.1016/j.ijheatmasstransfer.2016.06.042.

[121] Y. C. Hu, Q. Zhou, H. M. Ye, Y. F. Wang, and L. S. Cui, "Peculiar surface profile of poly(ethylene oxide) film with ring-like nucleation distribution induced by Marangoni flow effect," *Colloids Surfaces A Physicochem. Eng. Asp.*, vol. 428, pp. 39–46, 2013, doi: 10.1016/j.colsurfa.2013.03.035.

[122] G. McHale, S. M. Rowan, M. I. Newton, and M. K. Banerjee, "Evaporation and the wetting of a low-energy solid surface," *J. Phys. Chem. B*, vol. 102, no. 11, pp. 1964–1967, 1998, doi: 10.1021/jp972552i.

[123] A. M. Cazabat and G. Guéna, "Evaporation of macroscopic sessile droplets," *Soft Matter*, vol. 6, no. 12, pp. 2591–2612, 2010, doi: 10.1039/b924477h.

[124] "Printed Electronics Market Size, Trends | Industry Forecast Report, 2025." [Online]. Available: https://www.grandviewresearch.com/industry-analysis/printed-electronics-market.